



doi:10.1016/j.gca.2004.01.019

Controls on iron-isotope fractionation in organic-rich sediments (Kimmeridge Clay, Upper Jurassic, southern England)

ALAN MATTHEWS,^{1,*} HELEN S. MORGANS-BELL,² SIMON EMMANUEL,^{1,†} HUGH C. JENKYN,² YIGAL EREL,¹ and LUDWIK HALICZ³¹Institute of Earth Sciences, Hebrew University of Jerusalem, 91904 Jerusalem, Israel²Department of Earth Sciences, University of Oxford, Parks Road, Oxford, OX1 3PR, United Kingdom³Geological Survey of Israel, 30, Malchei Israel Street, 95501 Jerusalem, Israel

(Received May 16, 2003; accepted in revised form January 22, 2004)

Abstract—This study explores the fractionation of iron isotopes ($^{57}\text{Fe}/^{54}\text{Fe}$) in an organic-rich mudstone succession, focusing on core and outcrop material sampled from the Upper Jurassic Kimmeridge Clay Formation type locality in south Dorset, UK. The organic-rich environments recorded by the succession provide an excellent setting for an investigation of the mechanisms by which iron isotopes are partitioned among mineral phases during biogeochemical sedimentary processes.

Two main types of iron-bearing assemblage are defined in the core material: mudstones with calcite \pm pyrite \pm siderite mineralogy, and ferroan dolomite (dolostone) bands. A cyclic data distribution is apparent, which reflects variations in isotopic composition from a lower range of $\delta^{57}\text{Fe}$ values associated with the pyrite/siderite mudstone samples to the generally higher values of the adjacent dolostone samples. Most pyrite/siderite mudstones vary between -0.4 and 0.1% while dolostones range between -0.1 and 0.5% , although in very organic-rich shale samples below 360 m core depth higher $\delta^{57}\text{Fe}$ values are noted. Pyrite nodules and pyritized ammonites from the type exposure yield $\delta^{57}\text{Fe}$ values of -0.3 to -0.45% . A fractionation model consistent with the $\delta^{57}\text{Fe}$ variations relates the lower $\delta^{57}\text{Fe}$ pyrite and siderite \pm pyrite mudstones values to the production of isotopically depleted Fe(II) during biogenic reduction of the isotopically heavier lithogenic Fe(III) oxides. A consequence of this reductive dissolution is that a ^{57}Fe -enriched iron species must be produced that potentially becomes available for the formation of the higher $\delta^{57}\text{Fe}$ dolostones. An isotopic profile across a dolostone band reveals distinct zonal variations in $\delta^{57}\text{Fe}$, characterized by two peaks, respectively located above and below the central part of the band, and decoupling of the isotopic composition from the iron content. This form of isotopic zoning is shown to be consistent with a one-dimensional model of diffusional-chromatographic Fe-isotope exchange between dolomite and isotopically enriched pore water. An alternative mechanism envisages the infiltration of dissolved ferrous iron from variable (high and low) $\delta^{57}\text{Fe}$ sources during coprecipitation of Fe(II) ion with dolomite. The study provides clear evidence that iron isotopes are cycled during the formation and diagenesis of organic carbon-rich sediments. Copyright © 2004 Elsevier Ltd

1. INTRODUCTION

The variations in stable-isotope abundances of the light elements have provided profound insight into the interactions between the geosphere, biosphere and hydrosphere. Stable-isotope abundances of intermediate-mass metallic elements are measurable at natural abundance levels using double-spike TIMS methods and multicollector, magnetic sector-inductively coupled plasma mass spectrometry (MC-ICP-MS) (e.g., Halliday et al., 1998; Beard and Johnson, 1999; Johnson and Beard, 1999; Maréchal et al., 1999; Belshaw et al., 2000; Zhu et al., 2000a; Anbar et al., 2001; Siebert et al., 2001). Understanding the links between the observations on natural assemblages and the experimental and theoretical basis underlying isotope fractionation is one of the fundamental goals of isotopic studies. Experimental, theoretical, and field-based studies indicate that the isotopic systems of the transition elements iron, copper, and molybdenum ($^{57}\text{Fe}/^{54}\text{Fe}$; $^{65}\text{Cu}/^{63}\text{Cu}$; $^{97}\text{Mo}/^{95}\text{Mo}$) are potentially sensitive recorders of abiotic and biologically

controlled redox phenomena in low-temperature marine sedimentary, oceanic hydrothermal, and continental subsurface environments (Beard et al., 1999, 2003a; Mandernack et al., 1999; Maréchal et al., 1999; Anbar et al., 2000, 2001; Polyakov and Mineev, 2000; Zhu et al., 2000a, 2002; Barling et al., 2001; Bullen et al., 2001; Matthews et al., 2001; Schauble et al., 2001; Siebert et al., 2001; Johnson et al., 2002, 2003; Maréchal and Albarède, 2002; Skulan et al., 2002; Croal et al., 2003; Roe et al., 2003; Anbar, 2004; Icopini et al., 2004; Welch et al., 2004).

Biogenic and inorganic redox processes, the sources of the iron in a particular setting (lithogenic Fe(III) oxides; reduced Fe(II) solutions), and the sequential history of iron mobilization and mass transfer, are among causal factors that can contribute to iron-isotope fractionation in low-temperature geological settings. Terrestrial igneous rocks are very homogenous in isotopic composition with values of about $\delta^{56}\text{Fe} = 0.00 \pm 0.05\%$ (relative to the UW-Madison average igneous standard; Beard and Johnson, 1999; Beard et al., 2003b). Lithogenic sources of Fe in the modern (oxygenated) earth, such as weathering products, continental sediments, river loads, and marine turbidites, have similar isotopic composition to the those of the igneous rocks and thus imply that weathering and sediment transport have a negligible fractionation effect in oxidized surficial en-

* Author to whom correspondence should be addressed (alan@vms.huji.ac.il).

† Present address: Department of Environmental Sciences and Energy Research, Weizmann Institute of Science, Rehovot, Israel.

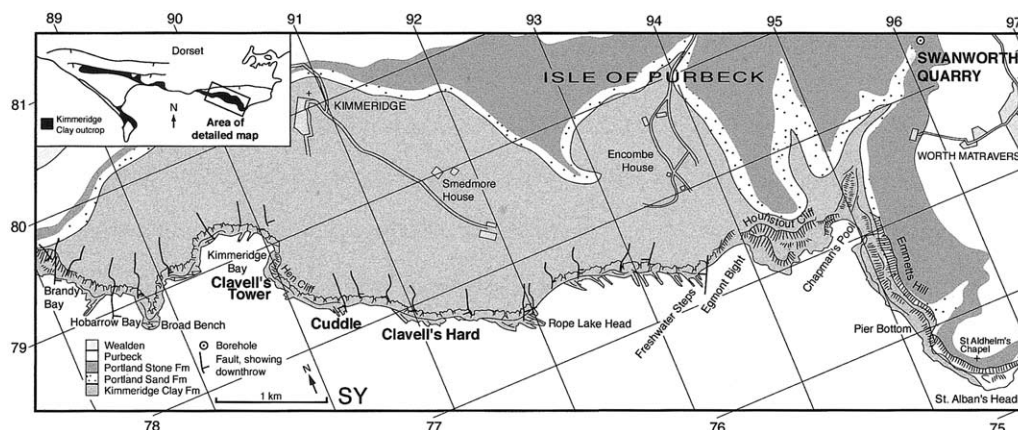


Fig. 1. Map showing the Kimmeridge Clay Formation outcrop near Kimmeridge in south Dorset, UK (after Morgans-Bell et al., 2001). Numbers around the edge of the map box refer to National Grid 10-km squares on Ordnance Survey Landranger Map sheets 194 and 195. Samples were collected from the Swanworth Quarry 1 borehole (located in the top-right hand corner of the map), and from the cliffs comprising the coastal section between Clavell's Tower and Cuddle (the Yellow Ledge Stone Band) and Clavell's Hard (the Blackstone).

vironments (Beard et al., 1999, 2003a,b). Chemically precipitated sediments on the other hand show marked variations in isotopic composition, revealed in studies of Quaternary Fe-Mn crusts in the northern Atlantic ocean (Zhu et al., 2000b), black shales (Beard et al., 2003b), Banded Iron Formations (Johnson et al., 2003), and low-temperature hydrothermal seafloor alteration (Sharma et al., 2001; Beard et al., 2003b; Rouxel et al., 2003). These examples potentially offer geochemical settings for understanding the processes that control iron-isotope fractionation in the natural environment.

This study investigates the fractionation of iron isotopes ($^{57}\text{Fe}/^{54}\text{Fe}$) in mineral phases from the organic-rich mudstones that comprise the Upper Jurassic (Kimmeridgian-Tithonian) Kimmeridge Clay Formation (KCF), at its type locality in south Dorset, UK (Fig. 1). Previous investigations of the KCF (e.g., Irwin et al., 1977; Scotchman, 1989; Macquaker et al., 1997), in common with other ancient organic-rich mudstones, have shown that its diagenetic evolution can be related to the depth-controlled reaction zones identified in modern sediments. These zones largely reflect thermodynamically and kinetically controlled sequences of reactions involving the bacterially mediated oxidation of the organic matter in anoxic conditions, beginning with the sulfate-reduction zone (SR), with or without anaerobic methane oxidation (AMO) at the base. Below these zones, fermentation reactions occur within the methanogenesis (Me) zone that, with increasing depth, transforms into the decarboxylation (D) zone where temperatures become too high for bacteria to persist (e.g., Claypool and Kaplan 1974; Froelich et al., 1979; Berner, 1980; Coleman, 1985; Curtis and Coleman, 1986; Curtis et al., 1986; Raiswell, 1987). Reduction of lithogenic Fe(III) iron oxides to dissolved ferrous iron may also occur in suboxic conditions in the Fe-reduction zone (FeR), allowing pyrite to form by reaction with H_2S generated by sulfate reduction either below the sediment-water interface or in stratified anoxic bottom waters (Berner, 1970, 1984; Canfield et al., 1996). Continued reduction of lithogenous iron and the uptake of dissolved Fe(II) in ferroan calcites and ferroan dolomites is thought to occur dominantly in the Me and D

zones (Irwin et al., 1977; Coleman, 1985; Curtis and Coleman, 1986; Scotchman, 1991).

The well-documented KCF organic-rich mudstone sequence, in which microbially mediated reduction processes play an important role, offers an excellent setting to study the way in which iron isotopes are partitioned between mineral phases in a microbially active sedimentary environment. The aim of this work is to characterize the iron-isotope compositions of the various iron-bearing phases in the KCF and to develop an understanding of the fractionation mechanisms that could control the isotopic partitioning. The study thus complements the growing body of experimental data on biogenic and abiogenic iron-isotope fractionations by exploring the mechanisms that can influence isotopic fractionation in a natural setting.

2. IRON-ISOTOPE FRACTIONATION AT SEDIMENTARY TEMPERATURES

Isotopic measurements of iron-isotope ratios have been carried out on both the $^{56}\text{Fe}/^{54}\text{Fe}$ ratio ($\delta^{56}\text{Fe}$) and $^{57}\text{Fe}/^{54}\text{Fe}$ ratio ($\delta^{57}\text{Fe}$ or $\epsilon^{57}\text{Fe}$). δ values are defined using the standard stable-isotope permil notation

$$\delta^{57}\text{Fe} = \left(\frac{^{57}\text{Fe}/^{54}\text{Fe}_{\text{sample}}}{^{57}\text{Fe}/^{54}\text{Fe}_{\text{standard}}} - 1 \right) \times 1000,$$

whereas $\epsilon^{57}\text{Fe}$ values are expressed relative to a standard in parts/10,000. Results expressed in the $\delta^{56}\text{Fe}$ notation are related to $\delta^{57}\text{Fe}$ by the theoretical mass-dependent fractionation relationship $\delta^{56}\text{Fe} = 0.68 \times \delta^{57}\text{Fe}$, which has been experimentally verified over a wide range of isotopic compositions (e.g., Matthews et al., 2001; Johnson et al., 2003).

Fractionations between two phases, A and B, are related to δ values by the relationship: $\Delta(A - B) = \delta A - \delta B \approx 1000 \ln \alpha_{A-B}$, where α_{A-B} is the fractionation factor (for $^{57}\text{Fe}/^{54}\text{Fe}$):

$$\alpha_{A-B} = \left(\frac{^{57}\text{Fe}/^{54}\text{Fe}}{^{57}\text{Fe}/^{54}\text{Fe}} \right)_A / \left(\frac{^{57}\text{Fe}/^{54}\text{Fe}}{^{57}\text{Fe}/^{54}\text{Fe}} \right)_B$$

Figure 2 summarizes fractionation data available at present for phases of interest to this study at temperatures of $\sim 25^\circ\text{C}$. The fractionations are presented for $\delta^{57}\text{Fe}$ and all data published

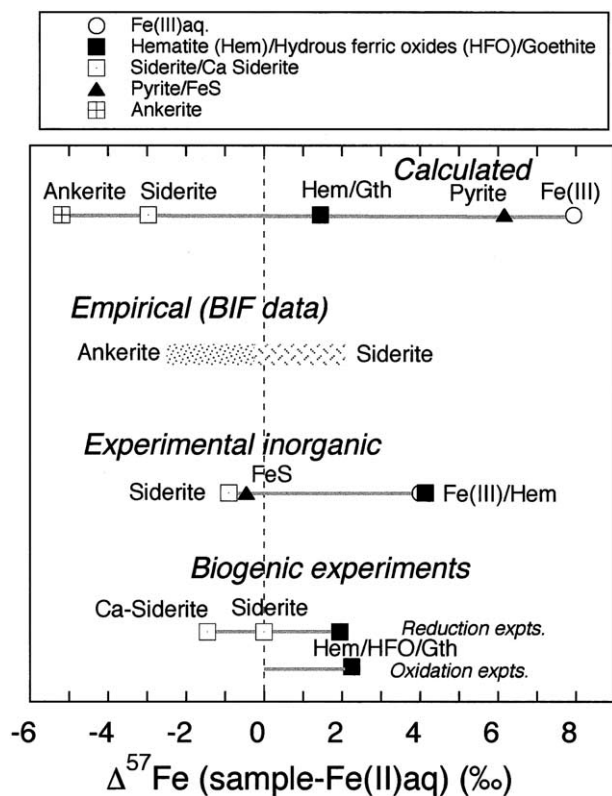


Fig. 2. Experimental iron-isotope fractionations at ca 25°C for various phases expressed relative to aqueous ferrous ion ($\Delta^{57}\text{Fe}$ (sample- Fe(II)aq)). Fractionation data reported using $^{56}\text{Fe}/^{54}\text{Fe}$ ratios have been converted to $^{57}\text{Fe}/^{54}\text{Fe}$ values. Data sources are as follows (refer to text for details): calculated, Polyakov and Mineev (2000) and Schauble et al. (2001); empirical (BIF) data, Johnson et al. (2003); experimental inorganic: Skulan et al. (2002), Johnson et al. (2002), Butler et al. (2003) and Wiesli et al. (2003); biogenic: Beard et al. (1999, 2003a), Icopini et al. (2004) and Croal et al. (2004) and Johnson et al. (2004); C. M. Johnson, personal communication.

using $\delta^{57}\text{Fe}$ values have been converted to $^{57}\text{Fe}/^{54}\text{Fe}$ ratios using the mass-dependent fractionation relation. Theoretical calculations of iron-isotopic fractionation using spectroscopic data by Polyakov and Mineev (2000) and Schauble et al. (2001) show that the heavier isotope is generally enriched in the oxidized iron species. This prediction was experimentally demonstrated in coprecipitation experiments for iron-isotope fractionation between Fe (III) and Fe (II) aqueous species at 22°C, where an $^{56}\text{Fe}/^{54}\text{Fe}$ fractionation of 2.75‰ was calibrated by Johnson et al. (2002). Subsequently, Welch et al. (2004) corrected this fractionation factor to $3.02 \pm 0.14\%$ (i.e., an $^{57}\text{Fe}/^{54}\text{Fe}$ fractionation of $\sim 4.5\%$) to allow for the effects of partial reequilibration during coprecipitation. Welch et al. (2004) also showed that this fractionation is temperature dependent, measuring a $^{56}\text{Fe}/^{54}\text{Fe}$ fractionation of $3.50 \pm 0.31\%$ at 0°C, and is unaffected by moderate variations in the chloride content in solution. An experimental determination of a near-zero fractionation between hexaquo Fe (III) ion and hematite at 98°C by Skulan et al. (2002) implies that these phases fractionate identically at 25°C. The iron-isotope fractionations from these experimental systems are significantly smaller than those theoretically predicted, but are consistent with more recent calcu-

lations of density function theory (Jarzecki et al., 2003; Anbar, 2004). Empirical estimates, based on iron-isotope fractionations among coexisting minerals in the Banded Iron Formation (BIF) of the Transvaal Craton (Johnson et al., 2003), show siderite and ankerite to be isotopically depleted minerals (Fig. 2). Theoretical calculations predict that pyrite is an isotopically heavy phase. However, the first results of an experimental study on the precipitation of FeS, which forms as a natural precursor mineral to pyrite (Canfield, 1989) show that it is isotopically depleted relative to the parent Fe(II) solution ($\Delta^{56}\text{Fe}(\text{FeS}-\text{Fe(II)}) = -0.3\%$; Butler et al., 2003). Abiogenically formed siderite is also indicated by experiment to be slightly isotopically depleted with respect to Fe(II) ion in solution (Wiesli et al., 2003).

In addition to the factors mentioned above, it has been shown that organic ligands may also influence isotope fractionation. Brantley et al. (2001, 2004) observed the formation of isotopically depleted Fe solution species during the dissolution of hornblende in the presence of organic Fe-chelating ligands, which they attributed to kinetic fractionation effects associated with formation of a leached surface layer. On the other hand, congruent solution is observed for goethite in the presence of organic ligands (Brantley et al., 2004), as previously was found for inorganic dissolution of hematite (Skulan et al., 2002).

Experimentally determined biogenic fractionations among iron isotopes are shown at the bottom of Figure 2. Aqueous Fe(II) ion formed during the action of dissimilatory Fe-reducing bacteria (*S. alga*) on hematite and hydrous ferric oxides (HFO) is approximately 1.3‰ depleted in ^{56}Fe (1.9‰ for $^{57}\text{Fe}/^{54}\text{Fe}$) relative to the solid (Beard et al., 1999, 2003a). Icopini et al. (2004) have observed a similar $^{56}\text{Fe}/^{54}\text{Fe}$ fractionation of -1.2% for goethite-Fe(II) in the presence of the reducing bacteria *S. putrefaciens*. In contrast, HFO formed by the action of photosynthetic Fe-oxidizing bacteria on Fe(II) in solution is isotopically enriched in ^{56}Fe by 1.3 to 1.5‰, equivalent to 1.9–2.2‰ in $^{57}\text{Fe}/^{54}\text{Fe}$ (Croal et al., 2004). Long-term experiments involving the formation of Fe carbonates by the dissolution of hydrous ferric oxide in the presence of dissimilatory Fe-reducing bacteria give $^{56}\text{Fe}/^{54}\text{Fe}$ fractionation factors of 0‰ for siderite-Fe(II) and -0.9% (-1.4% for $^{57}\text{Fe}/^{54}\text{Fe}$) for Ca-siderite-Fe(II) (Johnson et al., 2004; C. M. Johnson, personal communication). The smaller, experimentally measured biogenic aqueous Fe(III)-Fe(II) fractionations, relative to the inorganic equivalents, are taken to reflect the 'vital' effect of organisms long known from light stable-isotope geochemistry (Beard et al., 2003a). Thus, regardless of the mechanism, reduction is expected to result in isotopic depletion.

3. GEOLOGICAL SETTING OF THE KIMMERIDGE CLAY FORMATION AND SAMPLE LOCATIONS

The Kimmeridge Clay was deposited during Late Jurassic times within a north-south trending seaway that developed off the Laurasian continental margin (Whittaker, 1985; Ziegler, 1988, 1990; Bradshaw et al., 1992). The seaway connected the Boreal Sea with Tethys intermittently through the Jurassic, especially during times of high global sea-level, and the organic-rich facies that typify the Kimmeridge Clay today compose the primary oil-source rock for the North Sea Province. At its type locality in south Dorset (Fig. 1), the KCF consists of

~600 m of cyclic calcareous and organic-rich mudstones intercalated with coccolith limestones and dolostones. Here, the formation is immature having experienced only modest burial.

The stratigraphy of the KCF has recently undergone detailed reanalysis and description based upon a petrographical and mineralogical study of cores from three boreholes (two at Swanworth Quarry [SY 9675 7823] and one at Metherhills [SY 9112 7911]), drilled close to the coastal type section in Dorset. The work was carried out as part of the Natural Environment Research Council (NERC) Rapid Global Geological Events (RGGE) project “Anatomy of a Source Rock” (e.g., Gallois, 2000; Morgans-Bell et al., 2001). The study allowed a detailed characterization of the lithologies comprising the succession and found that creamy-white coccolith limestones and thin bands of iron-bearing limestones and dolostones intersperse four basic mudrock types (Morgans-Bell et al., 2001): (a) medium-dark to dark grey marl; (b) medium-dark to dark-grey-greenish-black shale; (c) dark-grey to greenish-black-olive black laminated shale; and (d) grayish-black–brownish-black mudstone, which constitute the most organic-rich rocks of the succession, with total organic-carbon (TOC) contents typically in the range 8–15 wt%. The most prominent horizon of lithological type (d) is the Blackstone (uppermost *wheatleyensis* zone) which, in the Swanworth Quarry 1 (SQ1) core, yields TOC contents >35 wt% (Morgans-Bell et al., 2001). At the type section, where the Blackstone commonly contains pyrite nodules over 10 cm in diameter (Fig. 3a), higher TOC values have been recorded, ranging from >35 to 63 wt% (Oschmann, 1988; Tyson, 1985, 1989; Myers and Wignall, 1987; Coe, 1992; Van Kaam-Peters et al., 1998; Sælen et al., 2000).

The variety of mudstone facies that make up the formation are thought to reflect changes in basin tectonics, sedimentation/burial rates of the different components, and variable oxygenation state of the bottom waters, which fluctuated from oxic to dysoxic/anoxic (e.g., Tyson et al., 1979; Wignall and Myers, 1988; Wignall and Newton, 1998; Raiswell et al., 2001). The presence of biomarkers sourced from green sulfur bacteria (isorenieratane derivatives) in KCF strata from the *wheatleyensis-pectinatus* zones, together with small (<5 µm), regular-sized pyrite framboids (*autissiodorensis-pectinatus* zones, Wignall and Newton, 1998), indicates that free H₂S was present in the water column and at least periodically extended into the photic zone (e.g., Sinnighe Damsté et al., 1998; Van Kaam-Peters et al., 1998). Sulfate reduction and pyrite precipitation hence took place at times well above the sediment-water interface. The bulk iron-isotope signatures of pyrite from the Kimmeridge Clay must therefore reflect the composition of material precipitated from dissolved ferrous iron within the water column as well as material remobilized within the sediment.

This study is based upon samples taken mainly from the Swanworth Quarry 1 core (see Fig. 4, after Morgans-Bell et al., 2001), with additional specimens collected from the type section in Dorset. The mudstone and stone band samples that comprise this study mostly range in age from the *autissiodorensis-hudlestoni* ammonite zones (spanning ~360–200 m depth in the SQ1 core, Fig. 4), and represent a relatively organic-rich part of the KCF. The stone bands are primarily ferroan dolostones, with the Basalt Stone Band (mid-*hudlestoni* zone) representing the only calcite-bearing stone band included

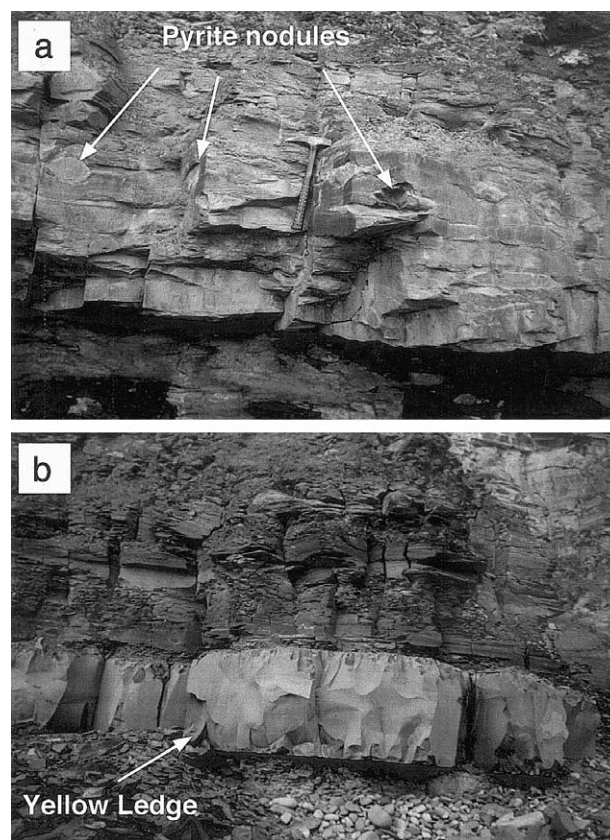


Fig. 3. Field photographs showing the cliff section comprising the Kimmeridge Clay Formation type section, illustrating (a) the organic-rich Blackstone (upper *wheatleyensis* zone) immediately east of Clavell’s Hard (SY 920 777), with constituent pyrite nodules indicated by arrows, and (b) the Yellow Ledge Stone Band (basal *scitulus* zone) near Cuddle (SY 912 782), which is a mustard yellow color in the field. Organic-rich mudstones occur above and below the stone band. A section through the stone band and adjacent mudstones was analysed by this study.

in the study. Note that the level of the Washing Ledge Stone Band (lower *autissiodorensis* zone) in the core is relatively weakly cemented and is likely only a poorly developed equivalent to that found at the coastal exposure. The bed is hence referred to herein as the Washing Ledge equivalent. It is worth noting that the carbonate stone bands intercalated within the KCF are more prominent in the weathered cliff section (Fig. 3b) than in the core, where they are most easily identified by their bell-like resonance on being struck with a hammer. The borehole samples consist of vertical slices of the central part of the core. The slices were divided into 10 cm intervals and powdered to give composite samples.

To obtain a good mineralogical specimen of pyrite for isotopic analysis, nodules of this mineral from the Blackstone (upper *wheatleyensis* zone) were sampled east of Clavell’s Hard (SY 920 777) at the type section. In addition, a pyritized ammonite was collected from organic-rich mudstones approximately 2 m below the Clavell’s Hard Stone Band (mid-*wheatleyensis* zone).

The iron-isotope distribution in the KCF ferroan dolostone bands was investigated through detailed measurements across

Swanworth Quarry 1 borehole

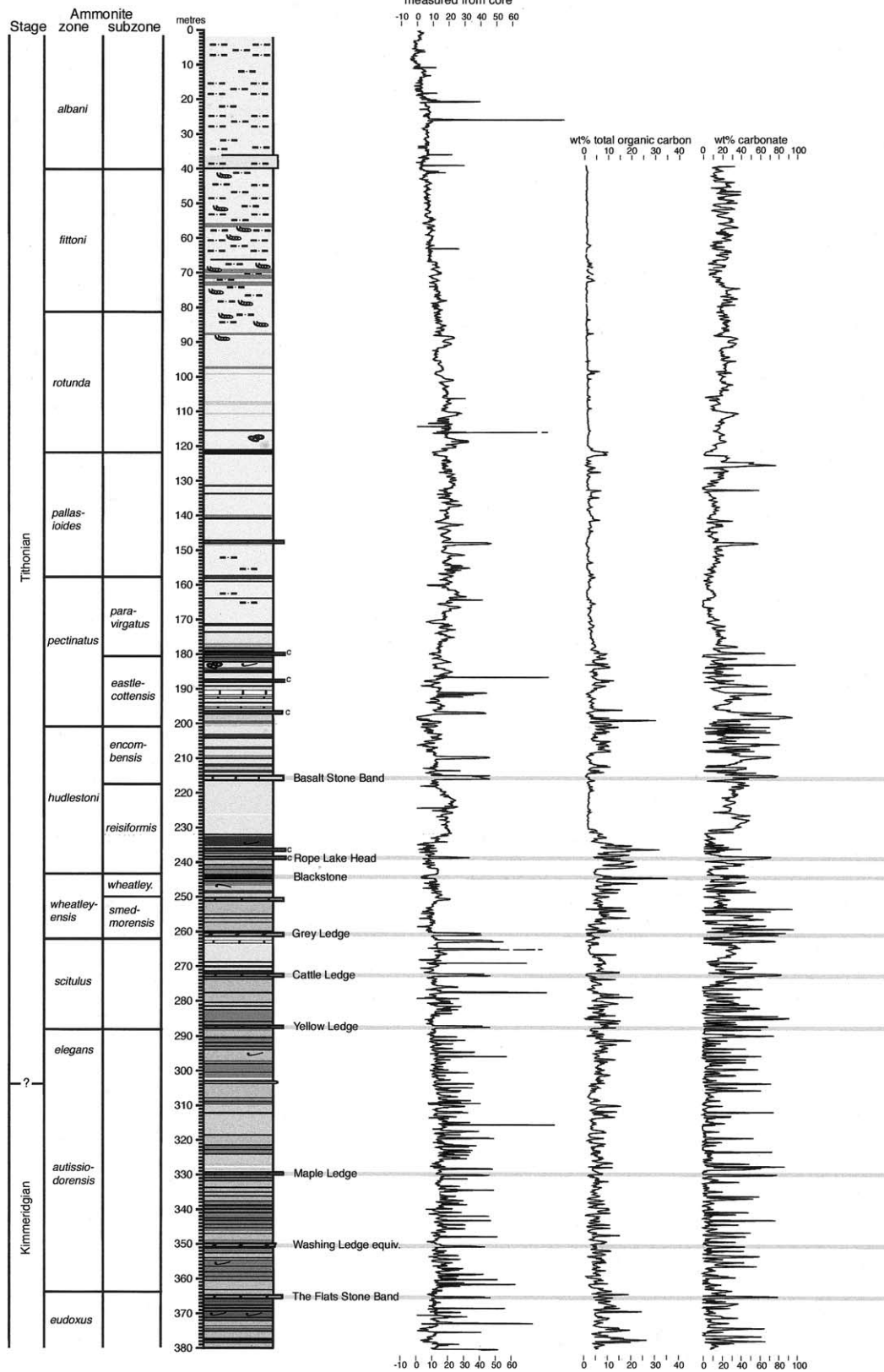


Fig. 4. Summary graphic log of the Swanworth Quarry 1 borehole (after Morgans-Bell et al., 2001). Composite samples from the core form the basis to this study. Ammonite zonation follows Cope (1967, 1978) and Cope et al. (1980); the stratigraphic position of the Kimmeridgian-Tithonian boundary is uncertain. The complete legend for the log can be found in Morgans-Bell et al. (2001). In general terms, the light gray tones shading the graphic log indicate calcareous mudstones, and the darker gray tones indicate shales and mudstones with higher organic-matter contents. The named stone bands are those measured in this study. The letter 'c' placed against some of the stone bands indicates those that are coccolith-rich. Magnetic susceptibility, total organic carbon, and carbonate data are shown alongside the graphic log (Morgans-Bell et al., 2001), and the stratigraphic positions of the named stone bands are indicated. The stone bands are characterized by high magnetic susceptibility values indicative of their iron-rich content.

the Yellow Ledge Stone Band (basal *scitulus* zone). A central slice of the 48-cm thick stone band and adjacent mudstones was acquired from the complete SQ1 core housed at the British Geological Survey (BGS) in Keyworth, UK. In addition to this study of the core, we also sampled the Yellow Ledge where it crosses the beach at the type section. Seven orientated, hand-sized specimens were taken from a 29-cm thick section of the stone band.

To complement the extensive database of Beard et al. (2003b) on lithogenic, oxidized (FeIII) iron source materials, we analysed several Mid-Upper Jurassic sedimentary iron (III) oxyhydroxides. These are: an Aalenian (~178 Ma) Fe-nodule from San Vigilio, northern Italy (Sturani, 1964); Bajocian (~174 Ma) ferruginous oncoliths from Burton Bradstock, Dorset (locally known as “snuffboxes”), a Kimmeridgian oolitic ironstone from Abbotsbury, Dorset, and a Tithonian (~150 Ma) ferruginous nodule from Tata, Hungary described by Fülöp (1976) (dates from Pálffy et al., 2000). The limonitic Bajocian ‘snuffboxes’ and Abbotsbury ironstone are suggested to have originally comprised layers rich in ferric iron oxyhydroxides that were wholly or partly replaced by chamosite/berthierine under reducing conditions during early diagenesis, but were later reconverted to goethite, perhaps under the influence of ground waters (Gatrall et al., 1972; Brookfield, 1973; Jones and Sellwood, 1989; Palmer and Wilson, 1990; Jenkyns and Senior, 1991). The other samples, from open-marine and pelagic sediments, are believed to have remained as oxyhydroxide phases throughout their history. Most lithogenous iron is carried down to the sea as ferric oxyhydroxides adhered onto clay particles (Carroll, 1958).

4. ANALYTICAL METHODS

The mineralogy of the composite samples from the SQ1 core was studied by X-ray powder diffraction (XRD) using an Philips Analytical X-ray Diffractometer. Magnetic susceptibility, total carbonate and TOC contents, and $\delta^{13}\text{C}$ (TOC) values were obtained from the detailed core log measurements (Morgans-Bell et al., 2001).

The samples of the Yellow Ledge Stone Band from the SQ1 core were sectioned at 2-cm intervals perpendicular to the core’s depth axis and portions of these slices were crushed to give a homogenous powder. Samples from the Yellow Ledge in the cliff section were also sectioned and cut at measured intervals and crushed to a powder.

The protocol for the preparation of Fe-solutions for iron isotopic analysis was modified after that used in the Department of Earth Sciences, University of Oxford (Zhu et al., 2002). Homogenized aliquots of 0.2 g sample were completely dissolved (total digestion) in Teflon beakers in ultrapure concentrated HCl, HF and 1:1 HClO₄, a stage that removes all silica and organic matter. The Fe content of the solution was determined by Atomic Absorption Spectroscopy and an appropriate amount of solution containing 100 μg Fe was placed in a Teflon beaker with a drop of 30% H₂O₂ and evaporated to dryness. The solid was then redissolved in 1 mL 6M HCl to produce a 100 ppm Fe solution for chromatographic separation using Biorad Macropore anion exchange resin MP1 100–200 mesh in its chloride form, which had been precleaned in 1M HCl and double dionized water (DDW) with the fine particles being decanted. Each sample was loaded onto the resin where Fe is preferentially taken up as $[\text{FeCl}_4]^-$ and further washed with 12 mL 6M HCl to remove unwanted ions (Ca, Mg, Al, etc). Elution of the Fe from the column was made by the addition of 11 mL 0.1M HCl in several aliquots. Under these conditions complete iron recovery is achieved from the columns.

The isotopic analyses were made using a sample bracketing method using a standard solution (1000 ppm Fe in 1M HCl) prepared from the IRMM-14 Fe wire standard. before MC-IC-PMS analysis, 1 drop of 30% H₂O₂ was added to 0.5 mL of the IRMM-14 stock solution, which

was evaporated to dryness and dissolved in 50 mL 0.1 M HCl to produce a ferric ion working standard. Fe isotopic measurements were made on a Nu Instruments (Wrexham, Wales, UK) MC-ICP-MS at the Geological Survey of Israel, as described by Belshaw et al. (2000) and Zhu et al. (2002). Sample and standard Fe-solutions were introduced at 10 ppm concentration to the plasma through a desolvating nebulizer without N₂ flow to eliminate interferences associated with ArN and hydroxide species. All analyses reported here are given in the $\delta^{57}\text{Fe}$ notation relative to the IRMM-14 standard. Beard et al. (2003a) report a $\delta^{57}\text{Fe}$ IRMM-14 value of $-0.11 \pm 0.07\%$ relative to their average igneous Fe standard. Adjustment of our analyses to the $\delta^{56}\text{Fe}$ values of the Madison laboratory (and vice-versa) is therefore made by subtracting 0.11‰ from our $\delta^{57}\text{Fe}$ (IRMM) values to give the $\delta^{57}\text{Fe}$ value relative to the average igneous standard, and then multiplying this value by 0.68.

A number of factors are known to influence the accuracy of iron-isotope analyses. These have been documented in detail by Belshaw et al. (2000), Zhu et al. (2002) and Beard et al. (2003a,b) and include both matrix and isobaric interferences. Several precautionary procedures and checks were made in this work to ensure the validity of the isotopic analyses.

1. Because of the high amounts of Ca and Mg in the sedimentary samples of this study, trace amounts of these elements were still found after one ion exchange column separation (Ca \leq 0.5 ppm; Mg \leq 0.2 ppm; Na \leq 0.4 ppm). Since ions such as Ca may potentially interfere with the mass spectrometry (Beard et al., 2003b), the chromatographic column separation procedure was repeated a second time. Chemical analyses of the resulting 10 ppm Fe solutions used in the mass spectrometry showed that these elements were below the analytical detection limits (\leq 0.1 ppm). The final eluted sample was evaporated to dryness with 1 drop 30% H₂O₂ to ensure all Fe is ferric (cf. Zhu et al., 2002, for a discussion of the valence effects on instrumental mass fractionation) and redissolved in 0.1M HCl to produce a 10 ppm solution for mass spectrometry. In addition to the precautions ensuring that both standard and sample contain iron that is entirely in the ferric state, MC-ICP-MS analysis was made within a few days of preparation of the 10 ppm Fe-solutions.

2. Mass spectrometric reproducibility was checked by running the IRMM-14 standard as both sample and standard (zero enrichment) and over the course of this study gave $\delta^{57}\text{Fe} = 0.00\%$ with a standard deviation of 0.04‰. A check of processing bias was made by the isotopic analysis throughout the study of IRMM-14 solution samples that were processed using the same double chromatographic separation protocol as for the KCF samples. This procedure gave $\delta^{57}\text{Fe} = 0.06\% \pm 0.09\%$ (1 σ).

3. Duplicate extractions of samples from this study were performed and replicate mass spectrometric analyses were made in different sessions (days). The analytical results from these checks are given in Table 1, together with the mean value and the standard deviation (1 σ) for each sample. These errors, together with those reported in above suggest that errors of \sim 0.1‰ (1 σ) are appropriate for this study. No correction has been made for the slightly positive average value of $\delta^{57}\text{Fe}$ (0.06‰) given by the chromatographic separation experiments on the IRMM-14 standard.

5. RESULTS

The results are given in Table 2, which lists the iron-isotope compositions together with sample depths for the composite samples taken from the SQ1 core and Fe wt% determined after total dissolution, estimated magnetic susceptibility, total carbonate and TOC content, and $\delta^{13}\text{C}$ TOC values.

5.1. Mineralogy of Iron-Bearing Phases

The results of the X-ray diffraction studies of the composite core samples are presented in Figure 5. They show that the mudstones consist mainly of calcite, clays (kaolinite and illite with minor palygorskite), and detrital minerals, with pyrite and/or siderite as the iron minerals. The stone bands are mostly

Table 1. Analytical replicates of samples analyzed in this study.

Sample	Rock type	Duplicate no. ^a	$\delta^{57}\text{Fe(I)}$ (‰)	Replicates ^b $\delta^{57}\text{Fe(II)}$ (‰)	$\delta^{57}\text{Fe(III)}$ (‰)	Mean $\delta^{57}\text{Fe}$ $\pm 1\sigma$ ‰
SQ1-92-2	Dolostone	92-2A	0.29	0.27		
		92-2B	0.27	0.30		
SQ1-100-30	Dolostone	100-30a	0.48	0.53	0.48	0.28 \pm 0.01
SQ1-109-26	Dolostone	109-26A	0.42	0.36		
		120-20B	0.37			
		120-20C	0.23			
SQ1-137-20	Dolostone	137-20A	0.14	0.17		0.50 \pm 0.03
SQ1-116-22	Mudstone	116-20A	-0.22	-0.18		0.39 \pm 0.03
		116-20B	-0.25			
		116-20C	-0.04			
SQ1-123-20	Mudstone	123-20A	-0.15	-0.20		0.28 \pm 0.07
SQ1-153-26	Mudstone	153-26A	0.51	0.49	0.53	0.16 \pm 0.02
		153-26B	0.43			
YL/-4	Mudstone	YL/-4A	-0.09	-0.04		-0.17 \pm 0.09
1-HUN	Fe-nodule	1A	0.85			-0.18 \pm 0.04
		1B	0.91			0.49 \pm 0.04
						-0.07 \pm 0.04
						0.88 \pm 0.04

^a Duplicate No (A,B etc) gives the number of duplicate chemical extractions of a sample.

^b Replicates give the results of MC-ICP-MS analyses of the sample made in different analytical sessions.

dolomite rich, with minor calcite, detrital minerals and clays. Pyrite is not indicated in these bands, with the exception of the Basalt Stone Band, which is calcite-dominated and contains pyrite, and the Washing Ledge equivalent, which contains prominent siderite in addition to pyrite, calcite and clays. The qualitative proportions of pyrite, siderite and dolomite, indicated by uncalibrated XRD peak heights, are plotted against depth in the lower diagram of the Figure 5. The antithetical relation between the dolomite-rich, but pyrite/siderite-absent stone bands, and the pyrite and/or siderite-bearing, dolomite-poor mudstones is clearly revealed. The iron mineralogy of composite samples can therefore be primarily assigned to pyrite and/or siderite in the mudstones (and beds such as the Washing Ledge equivalent) and to ferroan dolomite in the dolostone bands. The iron contents of the various composite samples show a positive correlation with magnetic susceptibility, consistent with the iron mineralogy (Fig. 6). Mudstone samples with pyrite as the only iron phase have Fe contents \sim 2.5 wt% and a low magnetic susceptibility characteristic of pyrite. Siderite \pm pyrite-bearing mudstone samples and ferroan dolomites have higher Fe contents (3–7 wt% and 4–6 wt%, respectively) and higher magnetic-susceptibility values in accordance with their higher paramagnetic susceptibility.

In a study of KCF mudstones from onshore and offshore (North Sea) locations, Macquaker et al. (1997) suggested that finite amounts of Fe(III) are substituted in clay minerals, principally octahedral sites of dioctohedral smectite. Illite and kaolinite are indicated to be the major clay minerals of the composite samples and Morgans-Bell et al. (2001) note that, in general, smectite and chlorite are present only in minor amounts in the core samples. Thus, while iron presence in the clay mineral structure cannot be eliminated, it is assumed to be a minor fraction of the total iron.

XRD studies of samples sectioned from the Yellow Ledge core sample show a uniform mineralogy across the stone band, dominated by dolomite with lesser calcite, and minor quartz and clay minerals. Trace amounts of residual pyrite were evident in SEM images.

5.2. Iron-Isotopic Compositions

The $\delta^{57}\text{Fe}$ values of the composite samples from the SQ1 core are plotted as a function of depth in Figure 7. A cyclic data distribution is apparent, which reflects variations in isotopic composition from a lower range of values associated with the pyrite/siderite mudstone samples to the generally higher values of the dolostone samples. Dolostones are isotopically enriched with respect to adjacent or nearby mudstones, with differences ($\Delta\text{Fe}(\text{dolostone-mudstone})$) varying from 0.1 to 0.8‰ (Fig. 7). Most pyrite/siderite mudstones vary between -0.4 and 0.1 ‰ whereas dolostones range between -0.1 and 0.5 ‰, although in samples below 360 m higher $\delta^{57}\text{Fe}$ values (~ 0.5 and 1.0 ‰, respectively) are noted. These stratigraphically lower samples are located in the very organic-rich shales of Bed groups 32 and 33 (after Morgans-Bell et al., 2001), representing the *eudoxus* zone, which have particularly high Fe contents of around 4 wt%. The average $\delta^{57}\text{Fe}$ values of samples above 360m depth are: pyrite-bearing mudstones (all samples, including those from the type exposure), -0.22 ± 0.20 ‰ (1σ); siderite/pyrite-bearing mudstones, -0.12 ± 0.06 ‰; dolostones, 0.32 ± 0.11 ‰. The isotopic composition of pyrite and siderite-bearing samples thus overlap within errors. No significant correlations were also evident between $\delta^{57}\text{Fe}$ and Fe content, TOC and $\delta^{13}\text{C}$ values (Table 2). Figure 7 also shows the range of $\delta^{57}\text{Fe}$ values of the 'lithogenic source' samples taken from the compilation of Beard et al. (2003b). The samples of Jurassic ferruginous oxyhydroxide crusts, nodules and oolites analysed in this study broadly overlap with this range, whereas the Tithonian ferromanganese nodule analysis yields a somewhat higher value of 0.88‰ (duplicate extractions).

The three samples of pyrite collected from the Blackstone and Clavell's Hard at the type section give $\delta^{57}\text{Fe}$ values of -0.31 to -0.45 ‰ (Table 1), falling in the lower end of the range of values for the pyrite-bearing mudstone samples. It is interesting to note that the composite core sample representing the Blackstone (box 102-sample 20) also gives $\delta^{57}\text{Fe}$ value of -0.31 ‰.

Table 2. Iron-isotope analyses of Kimmeridge Clay samples and Jurassic iron oxides.

Depth in core/m	Sample no.	Stone-band (SB) name	$\delta^{57}\text{Fe}$ (IRMM-14(‰))		Fe (wt%)	Magnetic susceptibility 10^6 SI	Total carbonate (wt %)	TOC wt%	$\delta^{13}\text{C}$ TOC	Sample notes ^a	
			Dolostones	Cc \pm siderite \pm pyrite mudstones							Fe(III) Oxides
Lithogenic Sources (Jurassic)											
	Ve1(Aalenian)				0.14					Fe-nodule, S. Vigillo, N. Italy	
	BJ-1(Bajocian)				0.16					Fe oncoliths ('Snuffboxes')	
	BJ-A (Bajocian)				0.42					Burton Bradstock, Dorset	
	AB-1 (Kimmeridgian)				-0.08					Limonic Ironstone, Abbotsbury, Dorset	
	1-HUN (Tithonian)				0.88					Ferromanganese nodule, Tata, Hungary	
SQ1 core 10 cm average samples											
119.60	SQ1-51-12				-0.09	3.4	22.5	14	1.1	-26.8	BG50, Pectinatus Nodules
213.95	SQ1-91-15				-0.39	2.3		36	6.6	-25.6	BG44, shale
215.18	SQ1-92-2	Unnamed SB	0.28			4.0	39.7	77	0.6	-26.4	Stone Band in BG44
216.49	SQ1-92-16	Basalt Stone	0.16			2.3	9.9	27	2.0	-26.9	Basalt Stone Band (Calcitic)
238.46	SQ1-100-30a	Rope Lake	0.50			3.6	32.5	72	4.3	-24.9	Rope Lake Head Stone Band
243.60	SQ1-102-20				-0.31	2.4	4.3	45	7.6	-24	Blackstone: Greyish Black-Brownish Black Mudstone with pyrite nodules
244.54	Sq1-103-1				-0.12	2.6	7.5	26	20.4	-25.9	Dark Grey-Greenish Black-Olive Black Shale (BG42)
245.00	SQ1-103-6				0.07	2.6	11.8	12	5.2	-25.7	Dark Grey-Greenish Black-Olive Black Shale (BG42)
254.58	SQ1-107-6				-0.11	2.5	2.7	13	6.3	-26.3	Med. Dark-Dark Grey Shale (BG41)
255.14	SQ1-107-12				-0.23	2.3	5.7	54	6.7	-25	Med. Dark Grey-Greenish Black Shale (BG41)
260.85	SQ1-109-26	Grey Ledge	0.39			3.9	40.8	81	0.9	-26.4	Grey Ledge Dolostone band
272.36	SQ1-114-21	Cattle Ledge	-0.10			3.6	33.9	82	0.7	-26.5	Cattle Ledge Dolostone band
277.24	SQ1-116-22				-0.17	7.0	72.6	2	5.7	-26.5	Med. Dark-Dark Grey Shale (BG38)
286.15	SQ1-120-10				0.08	2.7	9.3	4	11.9	-23.1	Dark Grey-Greenish Black-Olive Black Laminated Shale (BG37)
287.15	SQ1-120-20	Yellow Ledge	0.26			4.4	33.6	68	8.0	-23.3	Yellow Ledge Stone Band
294.60	SQ1-123-20				-0.18	4.3	36.3	30	7.1	-25.3	Med. Dark Grey-Greenish Black Shale (BG38)
327.65	SQ1-136-18				-0.08	2.5	14.1	21	1.6	-24.6	Med. Dark-Dark Grey Shale (BG35)
330.17	SQ1-137-20	Maple Ledge	0.16			5.8	45.0		1.6	-25	Maple Ledge Stone Band
350.70	SQ1-145-24	Washing Ledge			-0.03	6.2	35.2	45	3.5	-25.4	Washing Ledge Equivalent
361.34	SQ1-149-24				0.49	3.8	12.5	4	9.9		Med. Dark-Dark Grey Shale (BG33)
365.21	SQ1-151-6	The Flats	1.02				22.5	80	3.7		The Flats Stone Band
372.56	SQ1-153-26				0.49	3.9	22.5	10	7.8	-25.4	Med. Dark-Dark Grey Shale (BG32)
46 cm thick Yellow Ledge SB samples from SQ1 core*											
	YL/-4				-0.07	2.3					
	YL/0-2				0.03	5.2					
	YL/4-6		0.10			5.2					
	YL/10.5-12.5		0.27			4.8					
	YL/16-18		0.47			3.5					
	YL/22-24		0.00			3.0					
	YL/29-30		-0.14			3.7					
	YL/34-36		0.23			3.5					
	YL/40-42		0.06			3.9					
	YL/44-46		0.01			4.5					
	YL/51-52				-0.60	2.1					
29 cm thick Yellow Ledge SB exposure at Kimmeridge Bav ^b											
	YLE/0-1.5		-0.13				4.7				
	YLE/5.5-7.5		0.13			3.9					
	YLE/9.5-11.5		0.08			2.8					
	YLE/13.5-15.5		0.04			3.5					
	YLE/17-19		0.17			3.2					
	YLE/19.5-22		0.06			4.0					
	YLE/24.5-26		0.06			3.8					
	YLE/27-29		-0.23			4.7					
Pyrite from exposure at Kimmeridge Bay											
	BLN-A	Blackstone			-0.31						Pyrite nodule
	BLN-C	Blackstone			-0.45						Pyrite nodule
	CLN-1	2m below Clavell's Hard SB			-0.34						Pyritized ammonite

^a The location of the mudstone samples are given with respect to the Bed Groups (BG) defined by Morgans-Bell et al. (2001).^b Numbers after the YL/ refer to the position in cm from which the sample was sectioned and powdered. The distances are reported relative to the basal contact of the Stone Band.

Sample #	Lithological Type	Mudrock Type	anhydrite									
			kaolinite	palygorskite	illite	gyp./halite	feldspar	quartz	siderite	dolomite	calcite	pyrite
51-12	mudstone		2		2			4	1		4*	1
91-15	mudstone	a	2		2		1	3			4	1
92-2	BG44 SB		1	1	1			1		5		
92-16	Basalt SB		2		3	1	1	3		1	4	1
100-30	Rope Lake SB		1		1			2		4	3	
102-20	Blackstone	d	3	1	3			3			3	2
103-1	mudstone	c	1		2			3		1	3	2
103-6	mudstone	c	2		2	1		3		1	3	2
107-6	mudstone	b	2		3		1	3		1	3	2
107-12	mudstone	b	1		1			3			3	2
109-26	Grey Ledge SB		1		1			2		5	2	
114-2	Cattle Ledge SB		1		1		1	2		5		
116-22	mudstone	b	2	1	2	1	2	3	3			2
120-10	mudstone	c	3	1	3	2	1	4			2	3
120-20	Yellow Ledge SB		1		1			1		5	2	
123-20	mudstone	b	2	1	2		1	3	3		3	2
136-18	mudstone	b	3		2	2		3		1	2	1
137-20	Maple Ledge SB		1		1			2		4	1	
145-24	Washing L. Equiv.		3		3	1		2	3		2	1
149-24	mudstone	b	3		3	2	1	4			2	2
151-6	The Flats SB		1		1			1		5		
152-19	mudstone	b	3		3	2		3		1	1	2
153-26	mudstone	b	3		3	1	1	3	2	1	3	2

*contains aragonite

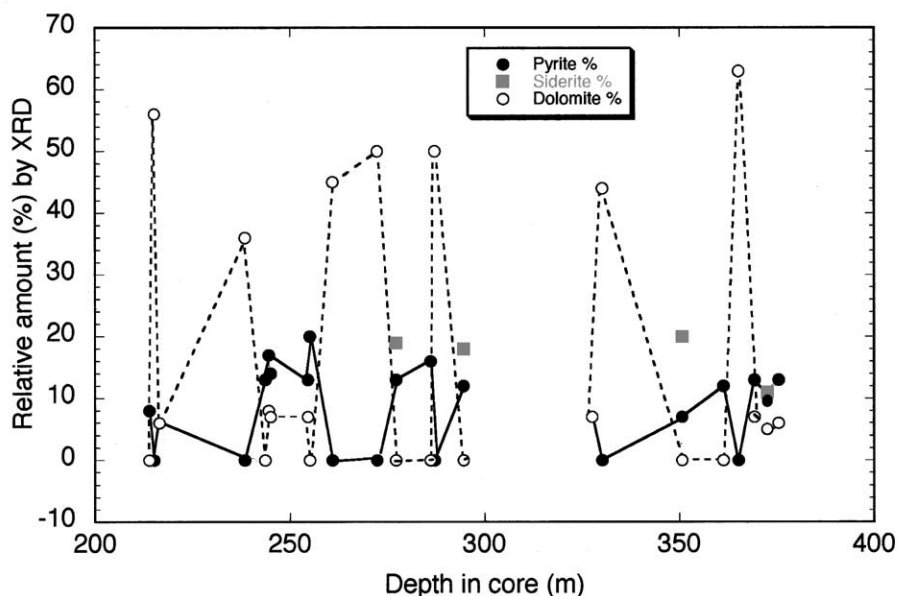


Fig. 5. Mineralogy of the Swanworth Quarry 1 composite samples. (a) Relative proportions of the minerals identified by X-ray diffraction search software are based on the relative heights of the major peaks. Sample numbers reflect SQ1 box and composite sample number, e.g., box 92, sample 16, for the Basalt Stone Band. (b) Relative proportions of dolomite, pyrite, and siderite as a function of depth in meters. Dolostone bands are recognizable by the "peaks" of dolomite abundance and alternate with the dolomite-poor, pyrite- and/or siderite-bearing samples.

The composite sample of the Yellow Ledge Stone Band gives an average $\delta^{57}\text{Fe}$ value of 0.28‰. The isotopic profiles across the Yellow Ledge and corresponding Fe contents in the core and exposure are plotted in Figure 8. Both profiles indicate decoupling of the $\delta^{57}\text{Fe}$ values from the iron content. This feature is most clearly revealed in a profile of samples sectioned from the core (Fig. 8a), where samples were taken at 2-cm intervals perpendicular to the depth axis; alternate slices were powdered and analysed. The profile reveals distinct, systematic zonal variations in $\delta^{57}\text{Fe}$ and Fe wt%. The $\delta^{57}\text{Fe}$ zoning is characterized by two peaks, located above and below the central part of the stone band. Taking the trend in the lower

half of the band as most clearly defining these changes, $\delta^{57}\text{Fe}$ values of around -0.1‰ in the centre rise to a maximum of $\sim 0.5\text{‰}$ some 18 cm from the margin before dropping to a value of $\sim 0\text{‰}$ at the lower (basal) margin. A similarly placed, but slightly smaller rise and fall of $\delta^{57}\text{Fe}$ values occurs within the upper part of the band. The $\delta^{57}\text{Fe}$ peaks thus appear to be positioned roughly symmetrically with respect to the centre and margins, with higher values occurring in the lower half. The iron contents show a different trend with the lowest values of around 3 wt% occurring in the centre, rising to maximum values of 4.5 to 5 wt% at the margins. The mudstone analyzed at 4 cm below the band (YL/-4) gives a $\delta^{57}\text{Fe}$ value of

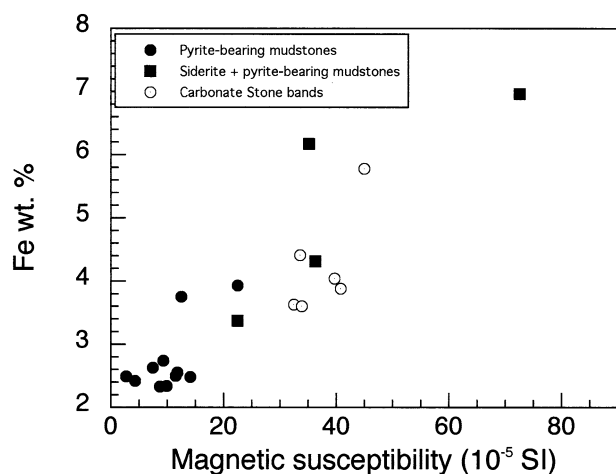


Fig. 6. A plot of wt% Fe of the SQ1 composite samples vs. magnetic susceptibility, determined from the core record for stone bands and pyrite- and siderite-bearing mudstones. Data from Table 2.

−0.07‰, whereas the sample from 4 cm above the band (YL/51-52) gives a value of −0.60‰, representing the lowest value measured in the mudstone samples.

The profile for the Yellow Ledge Stone Band sampled from the type exposure is given in Figure 8b. Although the variations in isotopic and Fe content variations are more muted, they still show features observed in the core sample; high $\delta^{57}\text{Fe}$ values in the interior decrease to lower values at the margin while Fe contents increase from centre towards the margins.

6. DISCUSSION

6.1. Iron-Isotope Composition of Mudstones

The depth vs. $\delta^{57}\text{Fe}$ profile for the composite samples from the SQ1 core show that the ferroan dolomites are isotopically-enriched with respect to the pyrite/siderite-bearing mudstones. This order of isotopic enrichment clearly disagrees with predictions of isotopic equilibrium based on the calculated fractionation factors (Fig. 2), which place pyrite as a markedly ^{57}Fe -enriched phase relative to both siderite and ankerite. The occurrence of pyrite as an isotopically depleted mineral phase has been observed in Banded Iron Formations (Johnson et al., 2003), with isotopic compositions among the lowest yet measured for natural materials. Experimental, empirical and theoretical studies of fractionations for carbonates indicate that ferroan dolomites should also be isotopically depleted relative to a lithogenic Fe(III) precursor (Fig. 2) and this is clearly not the case for the KCF samples.

Biogenic reduction processes form an isotopically depleted species relative to an Fe(III) source, and given the pivotal role of microbial processes in the organic-rich KCF mudstones, the formation of the pyrite/siderite from lithogenic iron sources can be examined from this standpoint. As discussed in Section 2, experimental data show that aqueous Fe(II) formed by the action of Fe-reducing bacteria on ferric oxides and hydroxides is approximately 1.8 to 1.9‰ depleted in ^{57}Fe relative to the solid at $\sim 25^\circ\text{C}$: (Beard et al., 1999, 2003a; Icopini et al., 2004). By contrast, $\Delta^{57}\text{Fe}(\text{siderite} - \text{Fe(II)}) = 0\%$ and for Ca-siderite

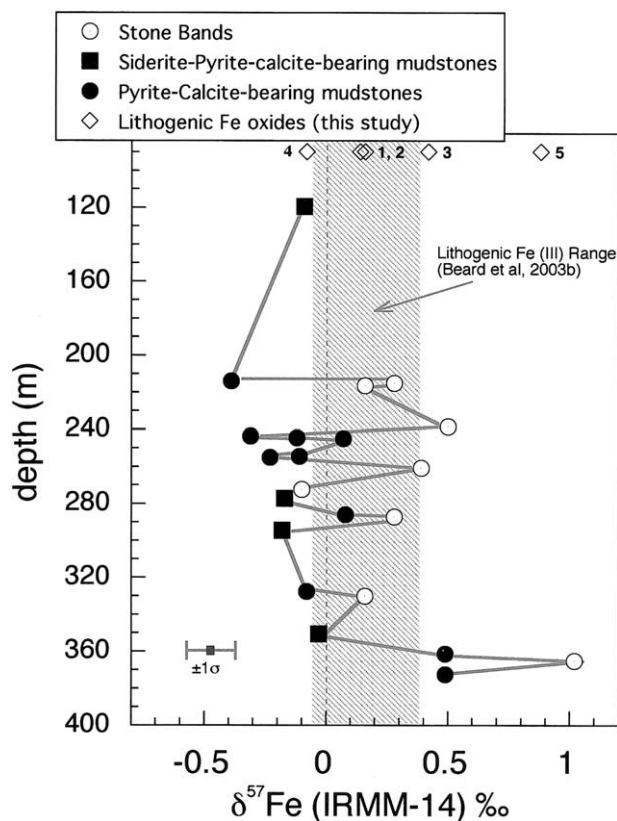


Fig. 7. $\delta^{57}\text{Fe}$ vs depth profile for the composite samples from the Swanworth Quarry 1 core. The shaded area shows the range of $\delta^{57}\text{Fe}$ analyses (expressed as the $\pm 2\sigma$ range after conversion to the IRMM standard) of lithogenic source materials given by Beard et al. (2003b) for clastic sedimentary materials including loess, aerosols, soil, modern oceanic turbidites, and the suspended load from rivers. The samples of Jurassic lithogenic iron oxyhydroxides analysed in this study are numbered: 1 = Aalenian Fe-nodule (San Vigilio, Italy); 2, 3 = Bajocian Fe-oncoliths (Burton Bradstock, Dorset); 4 = Kimmeridgian Fe-ooliths (Abbotsbury, Dorset); 5 = Tithonian ferromanganese nodule (Tata, Hungary).

(a possible analog for ferroan dolomite) $\Delta^{57}\text{Fe}(\text{Ca-siderite} - \text{Fe(II)}) = -1.4\%$ (Johnson et al., 2004; C. M. Johnson, personal communication). C and O isotope measurements of the carbonates of the Blackstone clearly define their origin in the sulfate-reduction (SR) zone (Irwin et al., 1977), with temperatures of calcite formation varying between 15 and 30°C . The $\delta^{57}\text{Fe}$ values of the pyrite samples from the Blackstone vary between −0.45 and −0.30‰ (Table 2). The $\delta^{57}\text{Fe}$ values of lithogenic source materials determined by Beard et al. (2003b) and the Jurassic iron oxides measured in this study (excepting the one high value for the Tithonian nodule) average $\sim 0.2\%$; thus the pyrite samples from the Blackstone are depleted by approximately 0.5 to 0.6‰ relative to this range. Other pyrite and siderite-bearing mudstone samples show similar or smaller differences (Fig. 7).

Given the data constraints noted above, the most straightforward model to account for the depleted isotopic compositions of the mudstone samples assumes that a variable component (pool) of low $\delta^{57}\text{Fe}$ Fe(II) forms in solution from dissimilatory Fe(III) reduction of oxides, followed by siderite and pyrite

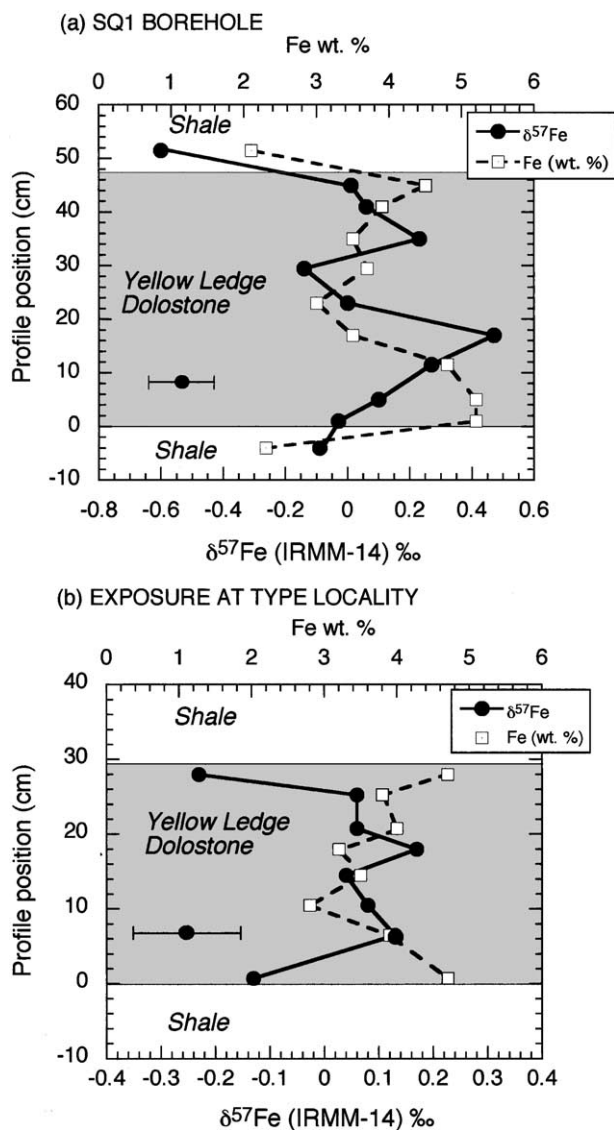


Fig. 8. Yellow Ledge Stone Band $\delta^{57}\text{Fe}$ and Fe wt% profiles. (a) Swanworth Quarry 1: profile of the 48 cm thick stone band, together with adjacent shales, sampled at 2-cm intervals. (b) Type locality exposure near Cuddle (SY 912 782): the 29 cm thick stone band sampled from 2 to 3 cm sections cut from aligned hand specimens collected from the exposed ledge. The data points are placed at the centre of each analyzed sample slice. All data are from Table 2. Errors are 1σ .

precipitation. Physically, this could take place either in the anoxic-euxinic bottom waters or below the sediment-water interface. The model is schematically illustrated for the SR zone in Figure 9 in which the dissolution of the ferric oxides is assumed to be congruent (Skulan et al., 2002; Brantley et al., 2004). Thus, Fe that is released into solution from the oxides as Fe(III) and then microbially reduced should give Fe(II) with initial $\delta^{57}\text{Fe} \sim 1.9\text{‰}$ lower than that of the Fe-oxide source. However, to create isotopically depleted Fe(II), an isotopically enriched intermediate Fe species must be formed at the same time to maintain isotopic mass balance, as noted by Johnson et al. (2003). Increased formation of Fe(II) from dissolution of the

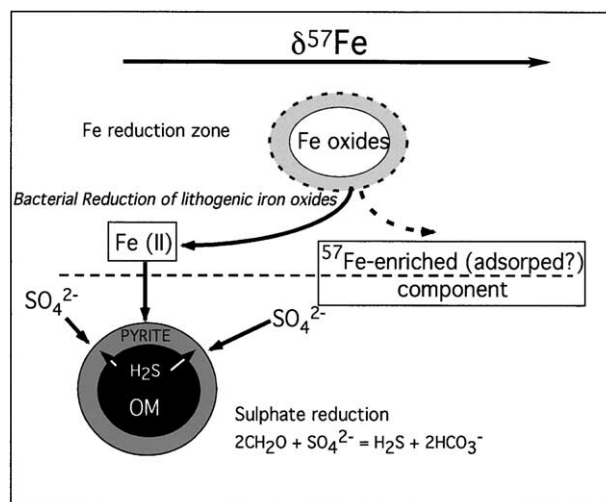


Fig. 9. Cartoon illustrating a potential fractionation mechanism for generating pyrite $\delta^{57}\text{Fe}$ values by bacterial reduction of lithogenic Fe oxides and hydroxides in the sulfate-reduction zone.

lithogenic Fe-oxide source and the enriched intermediate would increase the $\delta^{57}\text{Fe}$ value of the Fe(II), until at 100% conversion its $\delta^{57}\text{Fe}$ value would be equal to that of the original source material. The pyrites and siderites could thus form from pools or reservoirs of aqueous Fe(II) with variable $\delta^{57}\text{Fe}$. For siderite formation, Coleman (1993) and Coleman et al. (1993) have shown that biogenic mediation is essential for siderite growth by providing the source of carbonate through organic-matter oxidation and catalyzing Fe reduction. Thus, the siderite that forms biogenically from the Fe(II) pool is not expected to be fractionated ($\Delta^{57}\text{Fe}(\text{siderite-Fe(II)}) = 0$). Although the fractionation of biogenic pyrite-Fe(II) is not known, the first experimental data concerning inorganic FeS precipitation from Fe(II) solutions (Butler et al., 2003; Fig. 2) suggest that it may also be small. Thus, a small additional fractionation may accompany the formation of pyrite from solution Fe(II). Clearly, complete formation of pyrite and siderite from the available solution Fe(II) pool would result in no net fractionation.

The high $\delta^{57}\text{Fe}$ values of $\sim 0.5\text{‰}$ found in the lowermost sampled mudstones in the core, immediately beneath The Flats Stone Band within strata of the *eudoxus* zone, should reflect extensive conversion of lithogenic oxide source material to pyrite. Among the pyrite-bearing samples, these have the highest Fe content (Table 2), which could indicate the utilization of a large Fe(II) reservoir. Scotchman (1989) reported unusually heavy $\delta^{34}\text{S}$ values for the pyrites from these *eudoxus*-zone beds that he attributed to a depletion in the amount of sulfate during reduction. Significantly, such a depletion in sulfate is also consistent with an unusually large reservoir of iron.

Perhaps the greatest uncertainty of this model is the identity of the ^{57}Fe enriched intermediate. Possibilities are that oxidized Fe(III) forms as a separate solution pool or that rapid oxidation of Fe(II) produces isotopically enriched ferrihydrite (Bullen et al., 2001). Alternatively, in reducing conditions, ^{57}Fe -enriched Fe(II) forming in the sediments and/or bottom waters could become adsorbed by clays or onto mineral surfaces and provide a potentially labile reservoir of ^{57}Fe -enriched material. In the classic study of the role of clay minerals in the transportation of

iron, Carroll (1958) noted that marine black muds contain “ferrous oxides” (presumably oxyhydroxides) coexisting with amorphous ferrous sulfides. Furthermore, recent experimental studies of goethite dissolution in the presence of bacteria that secrete organic ligands show that formation of isotopically-light Fe in solution is driven by the bacterial uptake of isotopically-heavy Fe-organic complexes and possibly by adsorption onto goethite of isotopically heavy Fe (Brantley et al., 2004; S. L. Brantley, personal communication). Adsorption of isotopically-heavy Fe onto goethite has also been documented to be important during reductive dissolution of goethite by dissimilatory iron reducing bacteria under anaerobic conditions (Icopini et al., 2004). Most important is that the isotopically heavier intermediate could contribute to the higher $\delta^{57}\text{Fe}$ dolostones during later diagenesis.

6.2. Iron-Isotopic Zoning in the Yellow Ledge Stone Band

The carbonate stone bands are viewed as a form of laterally extended or coalesced concretionary carbonate growth (Coleman, 1993). Raiswell and Fisher (2000) distinguished two modes of growth based on cement textures: (i) concentric (or outward) growth where successive carbonate layers are added to the outer surface, increasing the radius (thickness) with time, and (ii) pervasive growth where the carbonate crystals simultaneously grow throughout the concretion volume and with little radius (thickness of the stone band) variation with time. Both growth mechanisms require porosity that can be filled by later cements, with the result that chemical or isotopic gradients across the concretionary bands may reflect changes in the relative proportions of early and later cements (Fisher et al., 1998; Raiswell and Fisher, 2000). Irwin et al. (1977) and Scotchman (1991) favored a concentric model, whereas Feistner (1989) showed that textural features of dolostone bands were consistent with pervasive growth.

Our mineralogical observations have indicated that the ferroan dolomites contain negligible amounts of pyrite, as illustrated in Figure 10, where the calculated stability fields of ferroan dolomite and pyrite as a function of pH and total sulfur ($\log S_T$) are plotted. Similar to siderite-FeS phase relations (Stumm and Morgan, 1996, their fig. 7.18), ferroan-dolomite stability over Fe^{2+} and pyrite is favored by increasing pH and low sulfur activity, respectively. Such conditions are consistent with the inference that the stone bands grew in reduced (methanogenic) conditions below the SR zone. Dolomite growth favored by high alkalinity and low sulfate activities has been suggested in a number of studies (e.g., Baker and Kastner, 1981; Hardie, 1987).

6.2.1. Diffusional Isotopic Exchange

The mechanism that leads to the observed offsetting of the $\delta^{57}\text{Fe}$ and Fe concentration peaks across the Yellow Ledge Stone Band (Fig. 8) is not immediately apparent. We first explore the potential role that diffusive transport might play during the diagenetic formation of the dolostones.

Because ^{57}Fe is not present in trace amounts ($^{57}\text{Fe}/^{54}\text{Fe} \sim 0.4$), diffusional models used to examine $\delta^{18}\text{O}$ in sedimentary systems, which assume that the heavier isotope is present in

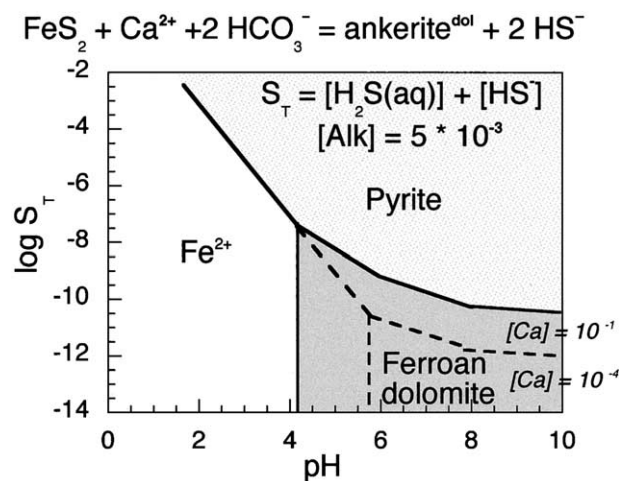


Fig. 10. Phase diagram illustrating the stability of ferroan dolomite with respect to pyrite and Fe^{2+} as a function of pH and $\log S_T$ (Total sulfur = $[\text{HS}^-] + [\text{H}_2\text{S}]$) at 25°C and 1 bar. The thermodynamic properties of ferroan dolomite are modelled in terms of its ankerite component assuming a fixed activity of 0.1. The equation illustrating the stability of this component with respect to pyrite is shown at the top of the diagram. The stability of the ferroan dolomite is given for two representative activities of Ca^{2+} in solution. The calculation method and equations defining alkalinity and $\log S_T$ are after Stumm and Morgan (1996, pp. 401–403). Data sources: ankerite (Holland and Powell, 1998); pyrite (Stumm and Morgan, 1996); solution species (Shock and Helgeson, 1988).

trace abundance (e.g., Burns, 1998), cannot be applied to the $^{57}\text{Fe}/^{54}\text{Fe}$ ratios and corresponding values of $\delta^{57}\text{Fe}$. Instead, we develop here an alternative diffusional model that potentially accounts for the pattern observed in the Yellow Ledge profile. As a close approximation, it will be assumed that the solid-aqueous partitioning of Fe between the solution and the dolomitic cement can be adequately described by dimensionless distribution coefficients (K_D^{Fe}):

$$K_D^{\text{Fe}} = \frac{(\text{Fe})_{\text{solid}}}{(\text{Fe})_{\text{aq}}} \quad (1)$$

where $(\text{Fe})_{\text{solid}}$ and $(\text{Fe})_{\text{aq}}$ are the solid and aqueous Fe concentrations respectively in moles per unit volume. As isotopic fractionation occurs during the exchange between aqueous Fe^{2+} and the mineral Fe^{2+} , distribution coefficients for each of the two isotopes can be defined:

$$K_D^{57\text{Fe}} = \frac{(^{57}\text{Fe})_{\text{solid}}}{(^{57}\text{Fe})_{\text{aq}}} \quad (2)$$

$$K_D^{54\text{Fe}} = \frac{(^{54}\text{Fe})_{\text{solid}}}{(^{54}\text{Fe})_{\text{aq}}} \quad (3)$$

From the definition of the fractionation factor, we obtain the following expression for solid aqueous partitioning

$$\alpha_{\text{solid-aq}} = \frac{(^{57}\text{Fe})_{\text{solid}} / (^{54}\text{Fe})_{\text{solid}}}{(^{57}\text{Fe})_{\text{aq}} / (^{54}\text{Fe})_{\text{aq}}} \quad (4)$$

and comparing to Eqns. 2 and 3, the following relationships are obtained:

Table 3. Boundary conditions for the diffusional model.^a

Time	Vertical distance (z)	⁵⁴ Fe concentration	⁵⁷ Fe concentration
t = 0	0 ≤ z ≤ ∞	0.1471	0.0563
t > 0	z = 0	1	0.3827
t > 0	z = ∞	0.1471	0.0563

^a Concentrations are indicated by arbitrary units. While the absolute values of the boundary concentrations influence the Fe concentration profiles, the $\Delta^{57}\text{Fe}$ profiles are only determined by the relative concentrations. The ratio of $^{57}\text{Fe}/^{54}\text{Fe}$ at $z = 0$ and $z = \infty$ is taken as the certified value for the IRMM - 14 standard (0.3827).

$$\alpha_{\text{solid-aq}} = \frac{(^{57}\text{Fe})_{\text{solid}} / (^{54}\text{Fe})_{\text{solid}}}{(^{57}\text{Fe})_{\text{aq}} / (^{54}\text{Fe})_{\text{aq}}} = K_{\text{D}}^{57\text{Fe}} / K_{\text{D}}^{54\text{Fe}} \quad (5)$$

and

$$K_{\text{D}}^{57\text{Fe}} = \alpha_{\text{solid-aq}} K_{\text{D}}^{54\text{Fe}} \quad (6)$$

In the case of iron-isotope partitioning between ferroan dolomite and Fe(II) in solution, α is less than unity (Fig. 2) and the distribution coefficient of ^{54}Fe should therefore be slightly greater than that of ^{57}Fe . If it is further assumed that the transport of aqueous Fe isotopes is effectively one dimensional and is determined only by solid-aqueous partitioning and vertical concentration gradients, the following two equations describing the spatial and temporal changes in aqueous Fe concentrations can be written for each isotope, adapted from the standard chromatographic equations described by Crank (1975):

$$\frac{\partial (^{57}\text{Fe})_{\text{aq}}}{\partial t} = \frac{D_{\text{Fe}}}{1 + K_{\text{D}}^{57\text{Fe}}} \frac{\partial^2 (^{57}\text{Fe})_{\text{aq}}}{\partial z^2} \quad (7)$$

$$\frac{\partial (^{54}\text{Fe})_{\text{aq}}}{\partial t} = \frac{D_{\text{Fe}}}{1 + K_{\text{D}}^{54\text{Fe}}} \frac{\partial^2 (^{54}\text{Fe})_{\text{aq}}}{\partial z^2} \quad (8)$$

where D_{Fe} is the effective diffusion coefficient for Fe in the porous matrix. Although not strictly correct, it is assumed that ^{57}Fe and ^{54}Fe diffuse at the same rate and that porosity is constant with time. Substituting Eqn. 6 into Eqn. 7 we obtain

$$\frac{\partial (^{57}\text{Fe})_{\text{aq}}}{\partial t} = \frac{D_{\text{Fe}}}{1 + \alpha_{\text{solid-aq}} K_{\text{D}}^{54\text{Fe}}} \frac{\partial^2 (^{57}\text{Fe})_{\text{aq}}}{\partial z^2} \quad (9)$$

With data on effective diffusion and distribution coefficients, (8) and (9) can readily be solved for different boundary conditions using analytical or numerical techniques. The equations have been solved here assuming a fixed boundary with a constant concentration, consistent with the boundary conditions of the pervasive-growth model. Solutions for the concentrations of each isotope were obtained using the analytical solution for a semi-infinite system with the boundary conditions indicated in Table 3. These model boundary conditions represent a system that is initially homogenous with respect to Fe concentration and isotopic composition and borders an infinitely large reservoir with higher aqueous Fe concentration but identical composition to the diffusional domain. Thus, the isotopic patterns that develop and diffuse through the system (the dolomite) are effectively driven by concentration gradients rather

than isotopic gradients. Such concentration gradients could form as a result of preferential dissolution of Fe-bearing minerals outside the diffusional domain. Importantly, as the isotopic profiles are determined by the relative concentrations of the boundary and initial conditions rather than the absolute values, arbitrary concentration units were used in the calculations. Using the solutions to the equations, isotopic profiles of different times may be obtained. In the following discussion, the Fe isotopic fractionation is defined by $\Delta^{57}\text{Fe}_{t-t_0}$, defined here as $\delta^{57}\text{Fe}$ at time = t minus $\delta^{57}\text{Fe}$ at time = 0. The advantage of this definition is that the curves reflect the change in the isotopic ratios of both the dolomite and aqueous species.

Clearly, the fractionation factor is a critical parameter of the modelling and the fractionation for Ca siderite-Fe(II) = -1.4‰ may serve as a good approximation for the biogenic fractionation between ferroan dolomite and Fe(II). As the theoretical and natural data for BIFs indicate (Fig. 2), ankerite should be depleted with respect to siderite. To explore the range of possibilities involving different fractionation factors, we have made calculations assuming three values of $\alpha_{\text{solid-aq}}$: 0.997, 0.998 and 0.999, corresponding to $\Delta^{57}\text{Fe}$ (dolomite-Fe(II)) values of -3, -2 and -1, respectively. These should cover the range of α values that might occur in both biogenic and abiogenic fractionation.

Calculated profiles of $\Delta^{57}\text{Fe}_{t-t_0}$ are illustrated in Figure 11a, demonstrating the way in which peaks of $\Delta^{57}\text{Fe}_{t-t_0}$ can develop within a profile and gradually move into the interior with time. Values chosen for the model parameters in this diagram are: $\alpha_{\text{solid-aq}} = 0.998$; $D_{\text{Fe}} = 5 \times 10^{-6} \text{ cm}^2\text{s}^{-1}$ (Li and Gregory, 1974); $K_{\text{D}}^{54} = 10^5$ (an Fe concentration in the dolomite of 4% by mass corresponds to an aqueous concentration of approximately $1-2 \times 10^{-5} \text{ M}$, consistent with values used to model the iron redox system (cf. Stumm and Morgan, 1996). It is interesting to note that the model peak overlaps the position of the peak observed in the Yellow Ledge after ~39,000 yr has elapsed. The model calculations thus illustrate that $\delta^{57}\text{Fe}$ patterns of the type shown in Figure 8a can develop and migrate in the ferroan dolomite bands as a result of diffusional isotopic exchange.

The various model parameters influence the profile shapes in different ways and a brief parametric analysis is shown in Figure 11b-e. Perhaps unsurprisingly, decreasing α by even relatively small degrees acts to amplify strongly the magnitude of the fractionation peak (Fig. 11b). Interestingly, while the K_{D} and D_{Fe} parameters determine the rapidity with which the isotopic peak moves through the system, both parameters have relatively little effect on the magnitude of the peak (Fig. 11c,d). By contrast, the initial concentration step at the boundary ($^{54}\text{Fe}_{\text{initial}} = ^{54}\text{Fe}_{\text{mudstone}} / ^{54}\text{Fe}_{\text{dolomite}}$) is found to be an important factor in determining the isotopic profile (Fig. 11e). In addition to influencing peak position, increasing the initial concentration step from 0.1 to 0.5 concentration units also considerably reduced the peak height.

A comparison of the isotopic data with model profiles demonstrates that a semiquantitative agreement can be obtained between the model and data from the Yellow Ledge (Fig. 12). Although too little data are currently available to successfully constrain boundary conditions and model parameters, the simulations nevertheless demonstrate that diffusional processes can reproduce the apparent decoupling of concentration peaks

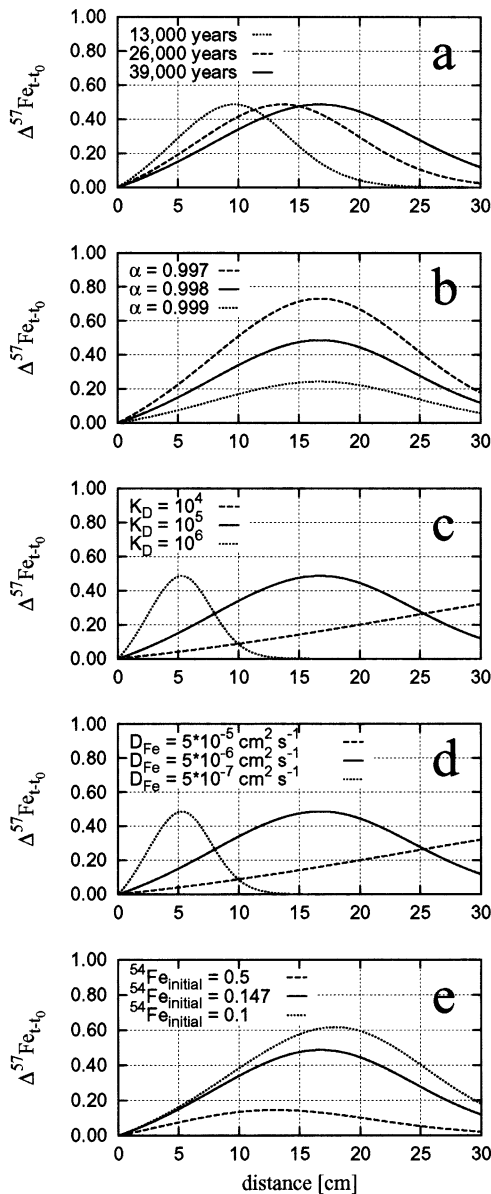


Fig. 11. Diffusion-model calculations of $\Delta^{57}\text{Fe}_{t-t_0}$ profiles. (a) Profiles at different times demonstrating the movement of the $\Delta^{57}\text{Fe}$ peaks towards the centre of the band. Boundary conditions are given in Table 3 and model parameters in the text. Simulated profiles at 39,000 yr are also shown for different values of (b) $\alpha_{\text{solid-aq}}$, (c) K_D , (d) D_{Fe} , and (e) $^{54}\text{Fe}_{\text{initial}}$.

from isotopic peaks. Thus, in addition to potentially accounting for pertinent features of the isotopic variations observed in the Yellow Ledge profile, the diffusional approach presented here could well be applicable to other diagenetic isotopic systems.

6.2.2. Variable $\delta^{57}\text{Fe}$ source reservoirs during dolostone growth

Advection of iron from variable $\delta^{57}\text{Fe}$ source reservoirs during the coprecipitation of Fe(II) with dolomite provides an alternative potential mechanism for changing isotopic composition during the growth of the dolostone bands. The increase in

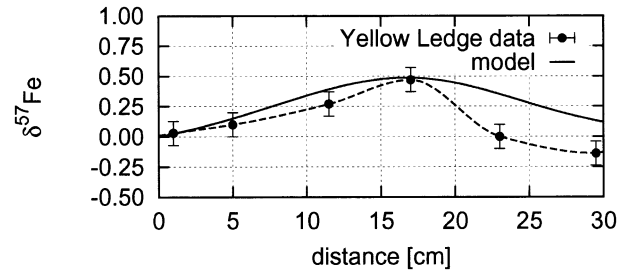


Fig. 12. Comparison of Yellow Ledge $\delta^{57}\text{Fe}$ data with a simulated profile based on model calculations. Model parameters in the simulation are those used in Figure 11a at 39,000 yr. Although relatively few constraints are available concerning the model parameters and boundary conditions, a qualitative similarity between the model and the measured profile can be seen.

$\delta^{57}\text{Fe}$ of the dolostone from the centre outward (Fig. 8a) could be accounted for by an increase in the flux of ^{57}Fe -enriched Fe(II) to the site of growing dolomite from a relatively large reservoir in the proximate mudstones. This flux could be supplied by the intermediate, possibly adsorbed, ^{57}Fe -enriched component that has been suggested to accompany the formation of pyrite and siderite. A second potential ^{57}Fe -enriched source could be provided by the dissolution of lithogenic iron oxides not utilized in the early diagenetic formation of pyrite and siderite.

As was noted earlier, the peak $\delta^{57}\text{Fe}$ values in the Yellow Ledge band are followed by a decrease in $\delta^{57}\text{Fe}$ toward the margins. In contrast, the Fe content continues to increase, reaching a maximum at the margins. This behavior suggests that, as growth continues, an additional component of ^{57}Fe -depleted aqueous Fe(II) is being added to the flux of iron during the later stages of dolostone growth. Theoretically, dissolution of framboidal pyrite in the mudstones hosting the stone bands could provide a low $\delta^{57}\text{Fe}$ source (Fig. 10); however, such a mechanism cannot be properly evaluated since the kinetics of such reactions are not known. An alternative source for the low $\delta^{57}\text{Fe}$ values is aqueous Fe (II) that is forming in other parts of the diagenetic column and advected to the site of dolostone growth.

An examination of the oxygen-isotope data of Irwin et al. (1977) shows that band centres generally have the highest $\delta^{18}\text{O}$ values, whereas low $\delta^{18}\text{O}$ values primarily occur in the margins of bands: a phenomenon they attributed to temperature increase during burial diagenesis. Increase in temperature may enhance the rate of dissolution and transport processes, hence accounting for the higher Fe contents at the margins of the dolostone bands.

7. CONCLUSIONS

A study of the $\delta^{57}\text{Fe}$ values of mudstones and dolomite bands in the organic-rich sediments of the Kimmeridge Clay Formation show that iron isotopes are mobilized and cycled, resulting in the partitioning of iron from lithogenic sources into lower $\delta^{57}\text{Fe}$ pyrites and siderite-bearing mudstones and higher $\delta^{57}\text{Fe}$ ferroan dolomite bands. Thus, in contrast to the rather low variation in the Fe-isotope compositions of oxidized (low-carbon) sedimentary rocks reported by Beard et al. (2003b),

organic carbon-rich sediments show isotopic evidence of redox changes and cycling. A simple fractionation model relates the formation of the lower $\delta^{57}\text{Fe}$ pyrite and siderite to variable degrees of reduction of lithogenic ferric oxide sources in a microbiologically active environment. A consequence of these fractionation processes that produce an isotopically depleted iron phase is that an ^{57}Fe -enriched intermediate iron species should be formed, which potentially may be utilized in the formation of the higher $\delta^{57}\text{Fe}$ values in dolostones.

Interpretation of the zoned isotopic distributions observed within a dolostone band suggests that both diffusional chromatographic processes and changing source reservoirs could contribute to the variation in the iron concentrations and iron-isotope compositions. Although we have examined these mechanisms separately, they are not mutually incompatible and more sophisticated models could be capable of integrating the two processes. Indeed, given that dolostone bands can form through both pervasive and concentric growth modes, these models are best regarded as potential end-member mechanisms for the fractionation of iron isotopes in the natural diagenetic situation.

The study demonstrates that the iron isotopic record of organic-rich sediments provides a powerful new tool for studying biogenically mediated sedimentary diagenetic processes.

Acknowledgments—This iron-isotope research was supported by the Israel Science Foundation (Grant 455/00). The Anatomy of a Source Rock project was funded by the NERC (Research grant numbers GST/02/1346 and GST/06/1346: Rapid Global Geological Events) and by a consortium of oil companies (Arco British, Conoco Norway, Enterprise, FINA, Phillips, Saga Petroleum, Shell, Statoil and Texaco). The Ministry of Defence and the Smedmore and Encombe estates kindly gave access to the cliffs near Kimmeridge. The British Geological Survey are thanked for providing access to the RGGE Kimmeridge Clay Cores. Nurith Vistowsky, and Reuben Belmaker are thanked for their help with the clean laboratory work and Dr. Irene Segal of the Geological Survey of Israel for her generous assistance with the mass spectrometry. Dr. C. M. Johnson and S. L. Brantley are thanked for kindly making available unpublished experimental data during the writing of the paper. The critical comments of Drs. C. M. Johnson, S. L. Brantley and R. Raiswell led to substantial revision of the manuscript and we would like to express our gratitude to these reviewers and to the Associate Editor, Dr. D. E. Canfield.

Associate editor: D. E. Canfield

REFERENCES

- Anbar A. D. (2004) Iron stable isotopes: Beyond biosignatures. *Earth Planet. Sci. Lett.* **217**, 223–236.
- Anbar A. D., Roe J. E., Barling J., and Nealon K. H. (2000) Nonbiological fractionation of iron isotopes. *Science* **288**, 126–128.
- Anbar A. D., Knab K. A., and Barling J. E. (2001) Precise determination of mass-dependent variations in the isotopic composition of Mo using MC-ICP-MS. *Anal. Chem.* **73**, 1425–1431.
- Baker P. A. and Kastner M. (1981) Constraints on the formation of sedimentary dolomite. *Science* **213**, 214–216.
- Barling J., Arnold G. L., and Anbar A. D. (2001) Natural mass-dependent variations in the isotopic composition of molybdenum. *Earth Planet. Sci. Lett.* **193**, 447–457.
- Beard B. L. and Johnson C. M. (1999) High precision iron isotope measurements of terrestrial and lunar materials. *Geochim. Cosmochim. Acta* **63**, 1653–1660.
- Beard B. L., Johnson C. M., Cox L., Sun H., Nealon K. H., and Aguilar C. (1999) Iron isotope biosignatures. *Science* **285**, 1889–1892.
- Beard B. L., Johnson C. M., Skulan J. L., Nealon K. H., Cox L., and Sun H. (2003a) Application of Fe isotopes to tracing the geochemical and biological cycling of Fe. *Chem. Geol.* **195**, 87–118.
- Beard B. L., Johnson C. M., Von Damm K. L., and Poulson R. L. (2003b) Isotope constraints on Fe cycling and mass balance in oxygenated earth oceans. *Geology* **31**, 629–632.
- Berner R. A. (1970) Sedimentary pyrite formation. *Am. J. Sci.* **268**, 2–23.
- Berner R. A. (1980) *Early Diagenesis: A Theoretical Approach*. Princeton University Press.
- Berner R. A. (1984) Sedimentary pyrite formation: An update. *Geochim. Cosmochim. Acta* **47**, 857–862.
- Belshaw N. S., Zhu X.-K., Guo Y., and O’Nions R. K. (2000) High precision measurement of iron isotopes by Plasma Source Mass Spectrometry. *Int. J. Mass Spectrom.* **197**, 191–195.
- Bradshaw M. J., Cope J. C. W., Cripps D. W., Donovan D. T., Howarth M. K., Rawson P. F., West I. M. and Wimbledon W. A. (1992) Jurassic. In *Atlas of Palaeogeography and Lithofacies* (eds. J. C. W. Cope, J. K. Ingram and P. F. Rawson), pp. 107–129. Memoir 13. Geological Society of London.
- Brantley S. L., Liermann L. J., and Bullen T. D. (2001) Fractionation of Fe isotopes by soil microbes and organic acids. *Geology* **29**, 535–538.
- Brantley S. L., Liermann L. J., Anbar A., Icopini G. A., Guynn R. L. and Barling J. (2004) Fe isotope fractionation during mineral dissolution with and without bacteria. *Geochim. Cosmochim. Acta*, in press.
- Brookfield M. E. (1973) The paleoenvironment of the Abbotsbury Ironstone (Upper Jurassic of Dorset). *Palaeontology* **16**, 261–274.
- Bullen T. D., White A. F., Childs C. W., Vivit D. V., and Schulz M. S. (2001) Demonstration of significant abiotic iron-isotope fractionation. *Geology* **29**, 699–700.
- Burns S. J. (1998) Can diagenetic precipitation of carbonate nodules affect pore-water oxygen isotope ratios? *J. Sed. Res.* **68**, 100–103.
- Butler I. B., Archer C., Rickard D., Vance D., and Oldroyd A. (2003) Fe isotope fractionation during Fe(II) monosulphide precipitation from aqueous solutions at pH 8 and ambient temperatures (abstract). *Geochim. Cosmochim. Acta* **67** (Suppl. 1), A51.
- Canfield D. E. (1989) Reactive iron in marine sediments. *Geochim. Cosmochim. Acta* **53**, 619–632.
- Canfield D. E., Lyons T. W., and Raiswell R. (1996) A model of iron deposition in euxinic Black Sea sediments. *Am. J. Sci.* **296**, 818–834.
- Carroll D. (1958) Role of clay minerals in the transportation of iron. *Geochim. Cosmochim. Acta* **14**, 1–27.
- Claypool G. E. and Kaplan I. R. (1974) The distribution and origin of methane in marine sediments. In *Natural Gases in Marine Sediments* (ed. I. R. Kaplan), pp. 99–139. Plenum Press.
- Coe A. L. (1992) Unconformities within the Upper Jurassic of the Wessex Basin, Southern England. D.Phil. thesis. Oxford University.
- Coleman M. L. (1985) Geochemistry of diagenetic non-silicate minerals: Kinetic considerations. *Phil. Trans. R. Soc. Lond. A* **315**, 39–56.
- Coleman M. L. (1993) Microbial processes; controls on the shape and composition of carbonate concretions. *Mar. Geol.* **113**, 127–4.
- Coleman M. L., Hedrick D. B., Lovely D. R., White D. C., and Pye K. (1993) Reduction of Fe(III) in sediments by sulphate-reducing bacteria. *Nature* **361**, 436–438.
- Cope J. C. W. (1967) The palaeontology and stratigraphy of the lower part of the Upper Kimmeridge Clay of Dorset. *Bull. Br. Museum (Nat. Hist.) Geol.* **15**, 3–79.
- Cope J. C. W. (1978) The ammonite faunas and stratigraphy of the upper part of the Upper Kimmeridge Clay of Dorset. *Palaeontology* **21**, 469–533.
- Cope J. C. W., Duff K. L., Parsons C. F., Torrens H. S., Wimbledon W. A., Wright J. K. (1980) *A Correlation of the Jurassic Rocks in the British Isles. Part 2: Middle and Upper Jurassic*. Special Report 15. Geological Society of London.
- Crank J. (1975) *The Mathematics of Diffusion*. 2nd ed. Oxford University Press.
- Croal L. R., Johnson C. M., Beard B. L. and Newman D. K. (2004) Iron isotope fractionation by anoxygenic Fe(II)-phototrophic bacteria. *Geochim. Cosmochim. Acta*, **68**, 1227–1242.

- Curtis C. D. and Coleman M. L. (1986) Controls on the precipitation of early diagenetic calcite, dolomite and siderite concretions in complex depositional sequences. In *Roles of Organic Matter in Sediment Diagenesis* (ed. D. L. Gautier), pp. 23–33. Special Publication 38, Society of Economic Paleontologists and Mineralogists.
- Curtis C. D., Coleman M. L., and Love L. G. (1986) Pore water evolution during sediment burial from isotopic and mineral chemistry of calcite, dolomite and siderite concretions. *Geochim. Cosmochim. Acta* **50**, 2321–2334.
- Feistner K. W. A. (1989) Petrographic examination and reinterpretation of concretionary carbonate horizons from the Kimmeridge Clay, Dorset. *J. Geol. Soc. Lond.* **146**, 345–350.
- Fisher Q. A., Raiswell R., and Marshall J. D. (1998) Siderite concretions from non-marine shales (Westphalian A) of the Pennines, England; controls on their growth and composition. *J. Sed. Res.* **68**, 1034–1045.
- Froelich P. N., Klinkhammer G. P., Bender M. L., Luedtke N. A., Heath G. R., Cullen D., and Dauphin P. (1979) Early oxidation of organic matter in pelagic sediments of the eastern equatorial Atlantic: Suboxic diagenesis. *Geochim. Cosmochim. Acta* **43**, 1075–1090.
- Fülöp J. (1976) The Mesozoic basement horst blocks of Tata. *Geol. Hungar.* **16**, 1–229.
- Gallois R. W. (2000) The stratigraphy of the Kimmeridge Clay (Upper Jurassic) in the RGGE Project boreholes at Swanworth Quarry and Metherhills, south Dorset. *Proc. Geol. Assoc.* **111**, 265–280.
- Gatral M., Jenkyns H. C., and Parsons C. F. (1972) Limonitic concretions from the European Jurassic, with particular reference to the “snuff-boxes” of southern England. *Sedimentology* **18**, 79–103.
- Halliday A. N., Lee D. C., Christiansen J. N., Rehkamper M., Li W., Luo X., Hall C. M., Ballentine C. J., Pettlee T., and Stirling C. (1998) Applications of multiple collector ICPMS to cosmochemistry, geochemistry and paleoceanography. *Geochim. Cosmochim. Acta* **62**, 919–940.
- Hardie L. A. (1987) Dolomitization: A critical review of some current views. *J. Sed. Petrol.* **57**, 166–183.
- Holland T. J. B. and Powell R. (1998) An internally consistent thermodynamic data set for phases of petrological interest. *J. Metam. Geol.* **16**, 309–343.
- Icopini G. A., Anbar A. D., Ruebush S. S., Tien M. and Brantley S. L. (2004) Iron isotope fractionation during microbial reduction of iron: The importance of adsorption. *Geology* **32**, 205–208.
- Irwin H., Curtis C., and Coleman M. (1977) Evidence for source of diagenetic carbonates formed during the burial of organic-rich sediments. *Nature* **269**, 209–213.
- Jarzecki A., Anbar A. D., and Spiro T. (2003) Iron isotope fractionation between $\text{Fe}(\text{H}_2\text{O})_6^{2+}$ and $\text{Fe}(\text{H}_2\text{O})_6^{3+}$ (abstract). *Geochim. Cosmochim. Acta* **67** (Suppl. 1), A187.
- Jenkyns H. C. and Senior J. R. (1991) Geological Evidence for intra-Jurassic faulting in the Wessex Basin and its margins. *J. Geol. Soc. Lond.* **148**, 245–260.
- Johnson C. M. and Beard B. L. (1999) Correction of instrumentally produced mass fractionation during isotopic analysis of Fe by thermal ionization mass spectrometry. *Int. J. Mass Spectrom.* **193**, 87–99.
- Johnson C. M., Skulan J. L., Beard B. L., Sun H., Neilson K. H., and Braterman P. S. (2002) Isotopic fractionation between Fe(III) and Fe(II) in aqueous solutions. *Earth Planet. Sci. Lett.* **195**, 141–153.
- Johnson C. M., Beard B. L., Beukes N. J., Klein C., and O’Leary J. M. (2003) Ancient geochemical cycling in the earth as inferred from Fe isotope studies of Banded Iron Formations from the Transvaal Craton. *Contrib. Mineral. Petrol.* **144**, 523–547.
- Johnson C. M., Roden E. E., Welch S. A., Beard B. L. (2004) Experimental constraints on Fe isotope fractionation during magnetite and Fe carbonate formation coupled to dissimilatory hydrous ferric oxide reduction. *Geochim. Cosmochim. Acta*, in press.
- Jones L. E. and Sellwood B. W. (1989) Palaeogeographic significance of clay mineral distributions in the Inferior Oolite Group (Mid Jurassic) of southern England. *Clay Minerals* **24**, 91–105.
- Li Y.-H. and Gregory S. (1974) Diffusion of ions in seawater and deep sea sediments. *Geochim. Cosmochim. Acta* **38**, 703–714.
- Macquaker J. H. S., Curtis C. D., and Coleman M. L. (1997) The role of iron in mudstone diagenesis: Comparison of Kimmeridge Clay Formation mudstone from Onshore and Offshore (UKCS) localities. *J. Sed. Res.* **67**, 871–878.
- Mandernack K. W., Bazylnski D. A., Hanks W. C., and Bullen T. D. (1999) Oxygen and iron isotope studies of magnetite produced by magnetic bacteria. *Science* **285**, 1892–1895.
- Maréchal C. L., Telouk P., and Albarède F. (1999) Precise analysis of copper and zinc isotopic compositions by plasma-source spectrometry. *Chem. Geol.* **156**, 251–273.
- Maréchal C. L. and Albarède F. (2002) Ion exchange fractionation of copper and zinc isotopes. *Geochim. Cosmochim. Acta* **66**, 1499–1509.
- Matthews A., Zhu X.-K., and O’Nions R. K. (2001) Kinetic iron stable isotope fractionation between iron (II) and iron (III) complexes in solution. *Earth Planet. Sci. Lett.* **192**, 181–192.
- Morgans-Bell H. S., Coe A. L., Hesselbo S. P., Jenkyns H. C., Weedon G. P., Marshall J. E. A., Tyson R. V., and Williams C. J. (2001) Integrated stratigraphy of the Kimmeridge Clay Formation (Upper Jurassic) based on exposures and boreholes in south Dorset, UK. *Geol. Mag.* **138**, 511–539.
- Myers K. J. and Wignall P. B. (1987) Understanding Jurassic organic-rich mudrocks—New concepts using gamma-ray spectrometry and palaeo-ecology: Examples from the Kimmeridge Clay of Dorset and the Jet Rock of Yorkshire. In *Marine Clastic Sedimentology* (eds. J. K. Leggett and G. G. Zuffa), pp. 172–189. Graham and Trotman.
- Oschmann W. (1988) Kimmeridge Clay sedimentation—A new cyclic model. *Palaeogeogr. Palaeoclimat. Palaeoecol.* **65**, 217–251.
- Pálffy J., Smith P. L., and Mortensen J. K. (2000) A U-Pb and $^{40}\text{Ar}/^{39}\text{Ar}$ timescale for the Jurassic. *Can. J. Earth Sci.* **37**, 923–944.
- Palmer T. J. and Wilson M. A. (1990) Growth of ferruginous oncoliths in the Bajocian (Middle Jurassic) of Europe. *Terra Nova* **2**, 142–147.
- Polyakov V. B. and Mineev S. D. (2000) The use of Mossbauer spectroscopy in stable isotope geochemistry. *Geochim. Cosmochim. Acta* **64**, 849–865.
- Raiswell R. (1987) Non-steady state microbiological diagenesis and the origins of concretions and nodular limestones. In *Diagenesis in Sedimentary Sequences* (ed. J. D. Marshall), pp. 41–54. Special Publication 36. Geological Society of London.
- Raiswell R. and Fisher Q. J. (2000) Mudrock-hosted carbonate concretions: A review of growth mechanisms and their influence on chemical and isotopic composition. *J. Geol. Soc. Lond.* **157**, 239–251.
- Raiswell R., Newton R., and Wignall P. B. (2001) An indicator of water-column anoxia: Resolution of biofacies variations in the Kimmeridge Clay (Upper Jurassic, UK). *J. Sed. Res.* **71**, 286–294.
- Roe J. E., Anbar A. D., and Barling J. E. (2003) Nonbiological fractionation of Fe isotopes: Evidence of an equilibrium isotope effect. *Chem. Geol.* **195**, 69–85.
- Rouxel O., Dobbek N., Ludden J., and Fouquet Y. (2003) Iron isotopic fractionation during ocean crust alteration. *Chem. Geol.* **202**, 155–182.
- Sælen G., Tyson R. V., Telnæs N., and Talbot M. R. (2000) Contrasting watermass conditions during deposition of the Whitby Mudstone (Lower Jurassic) and Kimmeridge Clay (Upper Jurassic) formations, UK. *Palaeogeogr. Palaeoclimatol. Palaeoecol.* **163**, 163–196.
- Schauble E. A., Rossman G. R., and Taylor P., Jr. (2001) Theoretical estimates of equilibrium Fe-isotope fractionations from vibrational spectroscopy. *Geochim. Cosmochim. Acta* **65**, 2487–2497.
- Scotchman I. C. (1989) Diagenesis of the Kimmeridge Clay Formation, onshore UK. *J. Geol. Soc. Lond.* **146**, 283–303.
- Scotchman I. C. (1991) The geochemistry of concretions from the Kimmeridge Clay Formation of southern and eastern England. *Sedimentology* **38**, 76–109.
- Sharma M., Polizzotto M., and Anbar A. D. (2001) Iron isotopes in hot springs along the Juan de Fuca Ridge. *Earth Planet. Sci. Lett.* **194**, 39–51.
- Shock E. L. and Helgeson H. C. (1988) Calculation of the thermodynamic and transport properties of aqueous species at high pressure and temperature: Correlation algorithms for ionic species and equation of state prediction to 5 kb and 1000°C. *Geochim. Cosmochim. Acta* **52**, 2009–2036.

- Siebert C., Nögler T. F. and Kramers J. D. (2001) Determination of molybdenum isotope fractionation by double-spike multicollector inductively coupled plasma mass spectrometry. *Geochem. Geophys. Geosyst.* **2**, 2000.GC00124.
- Sinninghe Damsté J. S., Kok M. D., Köster J., and Schouten S. (1998) Sulfurized carbohydrates: An important sedimentary sink for organic carbon? *Earth Planet. Sci. Lett.* **164**, 7–13.
- Skulan J. L., Beard B. L., and Johnson C. M. (2002) Kinetic and equilibrium Fe isotope fractionation between aqueous Fe(III) and hematite. *Geochim. Cosmochim. Acta* **66**, 2995–3015.
- Stumm W. and Morgan J. J. (1996) *Aquatic Chemistry: Chemical Equilibria and Rates in Natural Waters*. 3rd ed. Wiley-Interscience.
- Sturani C. (1964) La successione della fauna ad ammoniti nella formazioni mediogiurassiche delle Prealpi Venete Occidentali. *Mem. Ist. Geol. Mineral. Univ. Padova* **24**, 1–63.
- Tyson R. V. (1985) Palynofacies and sedimentology of some Late Jurassic sediments from the British Isles and northern North Sea. Ph.D. thesis. Open University.
- Tyson R. V. (1989) Late Jurassic palynofacies trends, Piper and Kimmeridge Clay Formations, UK onshore and northern North Sea. In *Northwest European Micropalaeontology and Palynology* (eds. D. J. Batten and M. C. Keen), pp. 135–172. Ellis Horwood.
- Tyson R. V., Wilson R. C. L., and Downie C. (1979) A stratified water column environmental model for the type Kimmeridge Clay. *Nature* **277**, 377–380.
- Van Kaam-Peters H. M. E., Schouten S., Köster J., and Sinninghe Damsté J. S. (1998) Controls on the molecular and carbon isotopic composition of organic matter deposited in a Kimmeridgian euxinic shelf sea: Evidence for preservation of carbohydrates through sulfuration. *Geochim. Cosmochim. Acta* **62**, 3259–3283.
- Welch S. A., Beard B. L., Johnson C. M. and Braterman P. S. (2004) Kinetic and equilibrium Fe isotope fractionation between aqueous Fe(II) and Fe(III). *Geochim. Cosmochim. Acta* **67**, 4230–4250.
- Whittaker A. (1985) *Atlas of Onshore Sedimentary Basins in England and Wales: Post Carboniferous Tectonics and Stratigraphy*. Blackie.
- Wiesli R. A., Beard B. L., and Johnson C. M. (2003) Experimental determination of Fe isotope fractionation between aq. Fe(II), “green rust,” and siderite (abstract). *Geochim. Cosmochim. Acta* **67** (Suppl. 1), A533.
- Wignall P. B. and Myers K. J. (1988) Interpreting benthic oxygen levels in mudrocks: A new approach. *Geology* **16**, 452–455.
- Wignall P. B. and Newton R. (1998) Pyrite framboid diameter as a measure of oxygen deficiency in ancient mudrocks. *Am. J. Sci.* **298**, 537–552.
- Zhu X.-K., O’Nions R. K., Guo Y., Belshaw N. S., and Rickard D. (2000a) Determination of natural Cu-isotope variation by plasma-source mass spectrometry: Implications for use in geochemical tracers. *Chem. Geol.* **163**, 139–149.
- Zhu X.-K., O’Nions R. K., Guo Y. L., and Reynolds B. C. (2000b) Secular variation of iron isotopes in North Atlantic Deep Water. *Science* **287**, 2000–2002.
- Zhu X.-K., Guo Y., Williams R. J. P., O’Nions R. K., Matthews A., Belshaw N., Canters G. W., de Waal E. C., Weser U., Burgess B. K., and Salvato B. (2002) Mass fractionation of the transition metal isotopes. *Earth Planet. Sci. Lett.* **200**, 47–62.
- Ziegler P. A. (1988) *Evolution of the Arctic-North Atlantic and the Western Tethys*. Memoir 43. American Association of Petroleum Geologists.
- Ziegler P. A. (1990) *Geological Atlas of Western and Central Europe*. 2nd ed. Shell International Petroleum BV, Maatschappij.